Low-dimensional chaos in the single wave model for self-consistent wave–particle Hamiltonian

Cite as: Chaos **31**, 083104 (2021); doi: 10.1063/5.0040939
Submitted: 17 December 2020 · Accepted: 14 July 2021 ·
Published Online: 2 August 2021

J. V. Gomes,[1,2,a] M. C. de Sousa,[2,3,b] R. L. Viana,[1,c] I. L. Caldas,[3,d] and Y. Elskens[2,e]

AFFILIATIONS

[1]Departamento de Física, Universidade Federal do Paraná, 81531-980 Curitiba, PR, Brazil
[2]Aix-Marseille Université, CNRS, PIIM UMR 7345, 13397 Marseille, France
[3]Universidade de Sao Paulo, Instituto de Fisica, 05508-090 São Paulo, SP, Brazil

[a]**Author to whom correspondence should be addressed:** janygovi@gmail.com
[b]**Electronic mail:** meirielenso@gmail.com
[c]**Electronic mail:** viana@fisica.ufpr.br
[d]**Electronic mail:** ibere@if.usp.br
[e]**Electronic mail:** yves.elskens@univ-amu.fr

ABSTRACT

We analyze nonlinear aspects of the self-consistent wave–particle interaction using Hamiltonian dynamics in the single wave model, where the wave is modified due to the particle dynamics. This interaction plays an important role in the emergence of plasma instabilities and turbulence. The simplest case, where one particle ($N = 1$) is coupled with one wave ($M = 1$), is completely integrable, and the nonlinear effects reduce to the wave potential pulsating while the particle either remains trapped or circulates forever. On increasing the number of particles ($N = 2$, $M = 1$), integrability is lost and chaos develops. Our analyses identify the two standard ways for chaos to appear and grow (the homoclinic tangle born from a separatrix, and the resonance overlap near an elliptic fixed point). Moreover, a strong form of chaos occurs when the energy is high enough for the wave amplitude to vanish occasionally.

Wave–particle interaction plays an important role in plasma dynamics both in the laboratory and in space. The processes resulting from the interaction between charged particles and waves are related to the emergence of instability and turbulence in plasmas. In phase space, this interaction can generate both regular trajectories, which may lead to coherent particle acceleration, and chaotic trajectories, which are responsible for particle heating and escape. Low-dimensional approximations often shed light on the dynamics of systems with many degrees of freedom, as chaotic motion arises as one increases the number of degrees of freedom. In the simplest case, one particle ($N = 1$) is coupled to one wave ($M = 1$) in a self-consistent way so that the wave is also modified due to the particle motion. This case is completely integrable so that all trajectories are regular and the nonlinear effects degenerate to particle trapping or circulating while the wave potential pulsates. The bifurcation diagram of this simple system displays a saddle-center coalescence and a special trajectory for which the wave intensity goes through zero. On increasing the number of particles ($N = 2$, $M = 1$), chaos arises as this Hamiltonian system is not integrable. For low energy, chaos appears due to nonlinear resonances near the elliptic fixed point. For moderate energy, chaos appears and becomes more intense in the homoclinic tangle associated with the hyperbolic fixed points. For high enough energy, the wave phasor can pulsate through zero, and the sudden jump in its phase induces large-scale chaos.

I. INTRODUCTION

Wave–particle interaction is one of the characteristic phenomena that occur naturally in plasma physics and play an essential role in their dynamics.[1,2] Plasmas are naturally conducive to the amplification and propagation of waves due to their intrinsic tendency to restore balance in the local distribution of charges when the system is exposed to disturbances.[3] Attempts to make plasmas return to equilibrium can excite a diversity of wave modes, which are able to propagate in the plasma and interact with particles whose velocities are close to their phase velocity.[4] Hamiltonian systems

provide a rich description of this interaction, where the regular and chaotic behavior of the particles trajectories in their phase space are directly related to the amplitude of the disturbance applied to the system.[5,6]

The exchange of energy and momentum through wave–particle interaction is especially important in rarefied plasmas where the collision time between charged particles is generally very long compared to the characteristic time scales of the system, and, therefore, those plasmas can be treated as non-collisional.[7] At first, this implies that, in practice, there is no energy dissipation in low-density plasmas since collisions are rare. However, the presence of waves can induce finite dissipation even in non-collisional plasmas:[8,9] plasma particles are scattered by the wave fields, and their energies and momenta change through such processes.

In general terms, effective finite dissipation in collisionless plasmas occurs via resonance and can give rise, for example, to the growth/damping of waves and heating/acceleration of particles, as well as to the transport of charged particles.[2,10,11] The interaction becomes stronger when the streaming velocity of the particles is such that the particle couples with the Doppler-shifted wave at its cyclotron frequency or its harmonics. This is the so-called cyclotron resonance interaction.[12] The special case of the Doppler-shifted wave frequency being zero (i.e., zero harmonic of the cyclotron frequency) corresponds to the well-known Landau resonance.[13]

In practice, Landau damping (respectively, growth) can be understood as follows: as observed experimentally,[14] particles with velocities slightly lower (larger) than the phase velocity of a wave are accelerated (decelerated) by the wave's electric field. Thus, particles that move a little slower (faster) than the phase velocity gain (lose) energy from (to) the wave.[15]

The main concepts described by Landau are widely used in particle accelerators to avoid instabilities in the coherent oscillation of the beams.[16] Besides, aspects of this interaction are notoriously important in space plasma physics, such as in the suprathermal electron acceleration at the solar wind,[17] in the interaction of charged particles with the Earth's magnetic field,[18] etc. For this reason, even many decades after its discovery,[19] there is high interest in the fundamental aspects related to Landau damping.[20,21]

An important feature of this type of interaction is that ions, being much more massive than electrons, are assumed to be fixed and their role is limited to providing charge neutrality for the system. The collective vibration of electrons with respect to ions is called Langmuir waves.[4] The usual description of the interaction of Langmuir waves with electrons whose velocities are close to their phase velocity involves the kinetic set of Vlasov–Poisson equations for the electron distribution function.[22]

In order to describe the interaction between charged particles and electrostatic waves, it is natural to use Hamiltonian models for which the particle dynamics in phase space generates both regular and chaotic trajectories.[5,6] The predominance of either type of trajectory depends mainly on the amplitude of the perturbation in the system that directly influences the particles motion.[23,24] In general, regions where regular trajectories prevail are more favorable to coherent particle acceleration, while chaotic regions are associated with particle heating and escape.[25]

Wave–particle interactions have often been described by Hamiltonian models in which particle motion is affected by the wave field, whereas the wave itself is not influenced by particle motion.[5,6] However, proper treatment of the problem would require also the addition of the wave response to the particle motion, which leads to so-called self-consistent Hamiltonians.[1,26] In this framework, the dynamics of Langmuir waves is described as M harmonic oscillators coupled to N quasi-resonant particles. Considering the single wave model (SWM) introduced by Onishchenko *et al.*[27] and O'Neil *et al.*,[28] it is possible to study the chaotic dynamics of wave–particle self-consistent interaction in terms of a few degrees of freedom. Indeed, this model can even be reduced to a four degrees of freedom system to describe its saturation regime,[29,30] and the model with a single particle was already considered by Adam *et al.*[31] with a view at its integrability and at the generation of sideband modes of the Langmuir waves.

The SWM originates from the description of the beam-plasma instability and has the advantage of behaving smoothly when the number of particles tends to infinity.[29,32] Since its introduction, this model has proven to be relevant in a variety of physical situations in which the dynamics is effectively dominated by a single mode as in the confinement of charged particles in tokamaks,[33] Landau damping,[34,35] free-electron lasers,[30,36] in the relationship between self-consistent chaos and phase space coherent structures,[37] and in kinetic instabilities of the Alfvén wave–particle interaction obtained experimentally in tokamak JET.[38]

In the present work, we revisit the dynamics of the single wave model with one particle ($N = 1$), which is integrable so that the phase portrait comprises only regular trajectories. The bifurcation diagram, in this case, shows a saddle-center coalescence that occurs for a specific value of total momentum P and divides the phase portrait topologies. Moreover, we stress the role of the trajectory for which the wave intensity I passes through zero, and we find a specific value of total momentum for which this trajectory coincides with a branch of the separatrix.

For two particles ($N = 2$), we study the emergence of low-dimensional chaos. We observe that the intensification of chaotic activity occurs both in the domains close to the elliptic fixed point and close to the separatrix associated with a hyperbolic fixed point. Fourier analysis shows that the nonlinear evolution of the particles motion, close to the elliptic fixed point, gives rise to the appearance and intensification of resonances. At higher energy, for which a hyperbolic point exists, the system is significantly chaotic. Moreover, for a still larger energy, the wave intensity can pass through zero, and the system exhibits chaos on a larger scale.

Our numerical computations were performed using a leap-frog symplectic integrator, which conserves the geometry of the system exactly and its energy quite accurately for long time.[39] For the non-integrable case with two particles, we studied the dynamics by intercepting the trajectories with a Poincaré section.[40]

This article is organized as follows: in Sec. II, we present the single wave Hamiltonian. The dynamics for one particle ($N = 1$) is revisited in Sec. III. General aspects of the two-particle model are discussed in Sec. IV. Fixed points and special trajectories are analyzed in Sec. V, while Sec. VI presents Poincaré sections and the

time evolution of typical trajectories. Section VII is devoted to our conclusions and prospects.

II. THE SINGLE WAVE HAMILTONIAN

The self-consistent dynamics of N identical particles moving on the interval of length L with periodic boundary conditions, interacting with M longitudinal waves with wave numbers $k_j = j2\pi/L$ and natural frequencies ω_{0j}, is described by the reference Hamiltonian[1,9]

$$H_{sc}^{N,M} = \sum_{r=1}^{N} \frac{p_r^2}{2m_r} + \sum_{j=1}^{M} \omega_{0j} \frac{X_j^2 + Y_j^2}{2} + \varepsilon \sum_{r=1}^{N} \sum_{j=1}^{M} k_j^{-1} \beta_j (Y_j \sin k_j x_r - X_j \cos k_j x_r), \quad (1)$$

$$H_{sc}^{N,M} = \sum_{r=1}^{N} \frac{p_r^2}{2m_r} + \sum_{j=1}^{M} \omega_{0j} I_j - \varepsilon \sum_{r=1}^{N} \sum_{j=1}^{M} k_j^{-1} \beta_j \sqrt{2I_j} \cos(k_j x_r - \theta_j), \quad (2)$$

where β_j is the coupling constant of wave j and ε is the overall coupling parameter. Here, $Z_j = X_j + iY_j = \sqrt{2I_j}\, e^{-i\theta_j}$, the generalized coordinates are the particles positions x_r and waves phases θ_j, and their conjugate momenta are the particles momenta p_r and waves intensities I_j. In phasor formulation, wave j has X_j as generalized coordinate with conjugate momentum Y_j.

Hamiltonian $H_{sc}^{N,M}$ comprises three contributions: the free motion (kinetic energy) of the particles, the (harmonic) oscillation of the waves, and the coupling between particles and waves. Besides that, Hamiltonian $H_{sc}^{N,M}$ is invariant under translation in time and in space so that the total energy $E = H_{sc}^{N,M}$ and the total momentum $P = \sum_{r=1}^{N} p_r + \sum_{j=1}^{M} k_j I_j$ are conserved. The latter constant reveals that the growth or decay of a wave is directly balanced with the slowing down or acceleration of particles.

We focus on a single special case, where all particles have the same mass, and we rescale time and energy to set the coupling constant $\varepsilon\beta_1$ and the particle mass m equal to unity in Eq. (3). In the single wave model ($M = 1$), we omit the subscript j and set the length unit to k^{-1} and the spatial period to $L = 2\pi$, which reduces the Hamiltonian to

$$H_{sc}^{N} = \sum_{r=1}^{N} \frac{p_r^2}{2} + \omega_0 I - \sqrt{2I} \sum_{r=1}^{N} \cos(x_r - \theta). \quad (3)$$

A Galileo transformation enables us to put the system in the reference frame of the wave. With the generating function $F_1(x, \theta, \bar{p}, \bar{I}, t) = \sum_{r=1}^{N} (x_r - \omega_0 t)(\bar{p}_r + \omega_0) + (\theta - \omega_0 t)\bar{I} - N\omega_0^2 t/2$, Hamiltonian (3) becomes

$$\bar{H}(\bar{p}, \bar{I}, \bar{x}, \bar{\theta}) = H_{sc}^{N} + \frac{\partial F_1}{\partial t}, = \sum_{r=1}^{N} \frac{\bar{p}_r^2}{2} - \sqrt{2\bar{I}} \sum_{r=1}^{N} \cos(\bar{x}_r - \bar{\theta}). \quad (4)$$

The total momentum

$$\bar{P} = \sum_{r=1}^{N} \bar{p}_r + \bar{I} \quad (5)$$

is conserved by the dynamics obtained from Eq. (4). This enables us to define a new generating function $F_2(\bar{x}, \bar{\theta}, p', I') = I'\bar{\theta} + \sum_{r=1}^{N} p_r'(\bar{x}_r - \bar{\theta})$: the new coordinate conjugate to $p_r' = \bar{p}_r$ is $x_r' = \partial F_2/\partial p_r' = (\bar{x}_r - \bar{\theta})$, which we denote as $y_r = x_r'$, and the new momentum conjugate to $\theta' = \bar{\theta}$ is $I' = \bar{P}$. The latter is a constant of motion so that the new angle $\theta' = \bar{\theta}$ is a cyclic coordinate. The final Hamiltonian, emphasizing that only N degrees of freedom are effective, is obtained in the compact form

$$H(p, y) = \sum_{r=1}^{N} \frac{p_r^2}{2} - \sqrt{2I} \sum_{r=1}^{N} \cos y_r, \quad (6)$$

where, for short, we dropped the prime from p_r' and the overbars from $\bar{I} = \bar{P} - \sum_r p_r'$ and from $\bar{H}$.

Wave–particle interaction is typical in many physical systems, and we investigate in this paper how this particular form of coupling given by Hamiltonian (6) affects the particle dynamics as we increase the number of degrees of freedom. This single wave Hamiltonian was first formulated as a simplified model to treat the instability due to a weak cold electron beam in a plasma, assuming a fixed ionic neutralizing background.[27,28] More recently, different studies extended the application of the single wave model to a much larger class of instabilities,[41] derived it in a generic manner from different contexts, and proved it could model various phenomena in fluids and plasmas,[37] and Compton free-electron laser amplification.[42]

III. THE SINGLE WAVE WITH ONE PARTICLE

In order to understand this system, we start with a few degrees of freedom. Following Adam, Laval, Mendonça, Tennyson, Meiss, Morrison, and del Castillo-Negrete and recalling results from Refs 29, 31, and 43, we first study the simplest, integrable case for this model where the self-consistency couples one particle and one wave, $M = N = 1$. As we will see in Sec. IV, the dynamics for $N = 2$ incorporates most of the basic phenomena that we will discuss in Secs. III A and III B. Moreover, the dynamics with $N = 1$ bears fundamental importance in the description of phenomena for the case with many particles,[29,31] where the macroparticle is used to describe the dynamics of an electron beam so that the beam electrons oscillate bunched at the bottom of the wave potential well during the trapping process.[27–30]

A. Preliminary analysis of the dynamics for $N = M = 1$

The single wave Hamiltonian for this case reads

$$H = \frac{p^2}{2} + (Y \sin x - X \cos x) = \frac{p^2}{2} - \sqrt{2I} \cos(x - \theta), \quad (7)$$

and the conserved total momentum is $P = p + I$. The evolution equations

$$\dot{x} = p, \tag{8a}$$

$$\dot{p} = -X\sin x - Y\cos x = -\sqrt{2I}\sin(x-\theta), \tag{8b}$$

$$\dot{X} = \sin x, \tag{8c}$$

$$\dot{Y} = \cos x \tag{8d}$$

imply that $\dot{X}^2 + \dot{Y}^2 = 1$ so that the wave never remains still. Besides, $\ddot{p} = -1 + (Y\sin x - X\cos x)p$.

For this simple case with only one particle, the single wave Hamiltonian has two degrees of freedom, one for the particle and one for the wave. As the Hamiltonian is invariant under space translations, the momentum conservation law reduces the problem to one degree of freedom. To express this, we introduce $y = x - \theta$ and write the Hamiltonian in the form

$$H = \frac{p^2}{2} - \sqrt{2(P-p)}\cos y, \tag{9}$$

with I expressed in terms of the particle momentum. As this Hamiltonian is time-independent, the system is completely integrable. In particular, particle orbits in phase portrait follow the constant energy contours ($H =$ constant).

The equations of motion of Hamiltonian (9) read

$$\dot{y} = p + \frac{1}{\sqrt{2(P-p)}}\cos y, \tag{10a}$$

$$\dot{p} = -\sqrt{2(P-p)}\sin y. \tag{10b}$$

The fixed points of the system are defined by the conditions

$$\dot{y} = \partial_p H = 0, \quad \dot{p} = -\partial_y H = 0. \tag{11}$$

Solving these conditions for Hamiltonian (9), we obtain the coordinates (y_i^*, p_i^*) of the fixed points C_i^*

$$C_1^* : \left(0, p_1^*\sqrt{2(P-p_1^*)} = -1\right), \tag{12a}$$

$$C_{2,3}^* : \left(\pi, p_{2,3}^*\sqrt{2(P-p_{2,3}^*)} = 1\right), \tag{12b}$$

with $p_1^* < 0$, $0 < p_2^* < 1$, $p_3^* > 1$, and the wave intensity at the fixed points given by $I_i^* = P - p_i^*$.

The stability of C_i^* is determined from the eigenvalues λ_i of the Jacobian matrix by linearizing the equations of motion (10a) and (10b) in the vicinity of each fixed point. Doing so, we find that the eigenvalues for C_1^* and $C_{2,3}^*$ are, respectively,

$$\lambda_1 = \pm\left(-\sqrt{2I_1^*} - \frac{1}{2I_1^*}\right)^{1/2}, \tag{13a}$$

$$\lambda_{2,3} = \pm\left(\sqrt{2I_{2,3}^*} - \frac{1}{2I_{2,3}^*}\right)^{1/2}. \tag{13b}$$

The eigenvalue λ_1 is imaginary for any value of I_1^*, which means that the fixed point $y_1^* = 0$ has elliptic stability. In addition, since $p_1^* < 0$, the physical condition $I_1^* = P - p_1^*$ implies that $I_1^* > P$ for any value of P.

When $I_2^* = I_3^* = 1/2$, the eigenvalues $\lambda_{2,3} = 0$, indicating a bifurcation point at $y_{2,3}^* = \pi$ that occurs for $P = 3/2$ and $p_2^* = p_3^* = 1$. For $I_2^* > 1/2$, the eigenvalue λ_2 is real so that in $y_2^* = \pi$ the system has hyperbolic stability for any $P > 3/2$ with $0 < p_2^* < 1$. Finally, for $0 < I_3^* < 1/2$, the eigenvalue λ_3 is imaginary, indicating that at the same abscissa $y_3^* = y_2^* = \pi$, we also have elliptic stability for any $P > 3/2$ with $p_3^* > 1$.

The values of p_i^* at the fixed points (12) are obtained as a function of total momentum P, i.e., $p_i^* = \pm 1/\sqrt{2(P-p_i^*)}$ so that we can describe the equilibrium solutions with the equation

$$(P - I_i^*)^2 I_i^* = 1/2. \tag{14}$$

As shown in Fig. 1, Eq. (14) selects the I_i^* values for which the cubic polynomial on the left-hand side assumes a given value. The blue (solid) line represents the stable solution at the elliptic fixed point at $y_1^* = 0$: this solution exists for any value of total momentum P. The black point at $P = 3/2$ shows a bifurcation, where two types of equilibria with different stabilities coincide at the same fixed position $y_{2,3}^* = \pi$. After the bifurcation point, the red (dotted) line corresponds to the unstable solution at the fixed position $y_2^* = \pi$, and the green (double-dotted) line corresponds to the stable solution in the same fixed position $y_3^* = \pi$.

The $M = N = 1$ system is integrable. Actually, solving (9) for $\cos y$ and squaring (8b) leads to the first order equation

$$\dot{p}^2 = 2(P-p)\left[1 - \left(\frac{H - p^2/2}{\sqrt{2(P-p)}}\right)^2\right]$$
$$= 2P - H^2 - 2p + Hp^2 - \frac{p^4}{4}, \tag{15}$$

which is solved analytically in terms of elliptic functions.[31] Briefly, one finds a function $\mathfrak{P}$ such that $p = \mathfrak{P}(t; p^*, P, H)$ by integrating (15), and a function $\mathfrak{Y}$ such that $y = \mathfrak{Y}(t; p^*, P, H) = \arcsin[-\dot{p}/\sqrt{2(P-p)}] = \arccos[(p^2 - 2H)/\sqrt{8(P-p)}]$ modulo boundary conditions. One can also construct action-angle variables for each type of periodic trajectory.

The equilibrium points $p = p_i^* =$ constant for Eq. (15) are defined by the conditions

$$G(p_i^*) = 0, \quad \left.\frac{\mathrm{d}G}{\mathrm{d}p}\right|_{p=p_i^*} = 0, \tag{16}$$

with $G(p)$ the quartic polynomial on the right-hand side of (15).

Solving (16) for the values of parameters H and P, we find parametrically given curves

$$P(p_i^*) = \frac{1 + 2p_i^{*3}}{2p_i^{*2}}, \quad H(p_i^*) = \frac{2 + p_i^{*3}}{2p_i^*}. \tag{17}$$

These curves on the (P, H) plane contain important information on the system dynamics.[44]

The loci of Eq. (17) on the (P, H) plane are shown in Fig. 2. As in Fig. 1(a), the blue (solid) curve represents the stable elliptic point at $y_1^* = 0$; the black point at $(P, H) = (3/2, 3/2)$ with

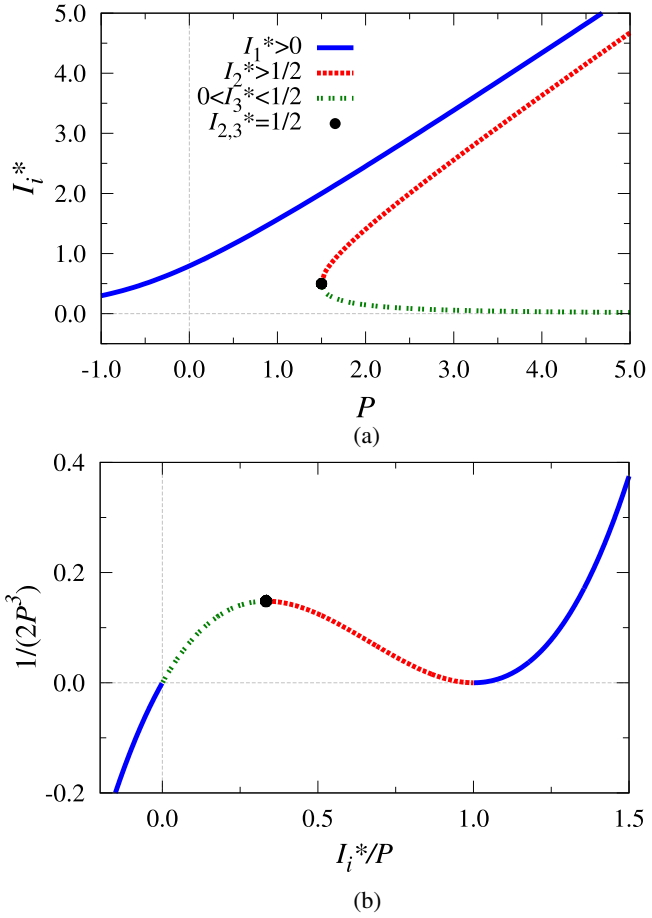

FIG. 1. (a) Bifurcation diagram of Eq. (14) for the $M = N = 1$ system. The blue (solid) line corresponds to the elliptic stable fixed point at $y_1^* = 0$. The black point at $I_{2,3}^* = 1/2$ and $P = 3/2$ corresponds to the bifurcation, and the red (dotted) and green (double-dotted) lines correspond, respectively, to the hyperbolic and the elliptic fixed points at $y_{2,3}^* = \pi$ after bifurcation. (b) Roots of the normalized equation (14), $(1 - I_i^*/P)^2 I_i^*/P = 1/(2P^3)$.

$p_{2,3}^* = 1$ corresponds to bifurcation; the red (dotted) curve represents the parameters of the hyperbolic fixed point at $y_2^* = \pi$; and the green (double-dotted) line is associated with the elliptic fixed point also at $y_3^* = \pi$. After bifurcation, for a given value of P, the energy of the stable (elliptic) fixed point at $y_1^* = 0$ is lower than the energy of the hyperbolic fixed point at $y_2^* = \pi$, and the latter, in turn, is lower than the energy of the elliptic fixed point at $y_3^* = \pi$. The topological changes described by the solutions of (14) in Fig. 1(a) and by (17) in Fig. 2 are presented in the phase portraits of Sec. III B.

Moreover, for (P, H) on these curves, the evolution equation (15) reduces to

$$\dot{p} = \pm(p - p^*)\left(\frac{1}{p^*} - \frac{(p - p^*)^2}{4}\right)^{1/2}, \tag{18}$$

which can be solved in terms of elementary functions. Specifically, if $0 < p^* < 1$, this equation admits real-valued solutions

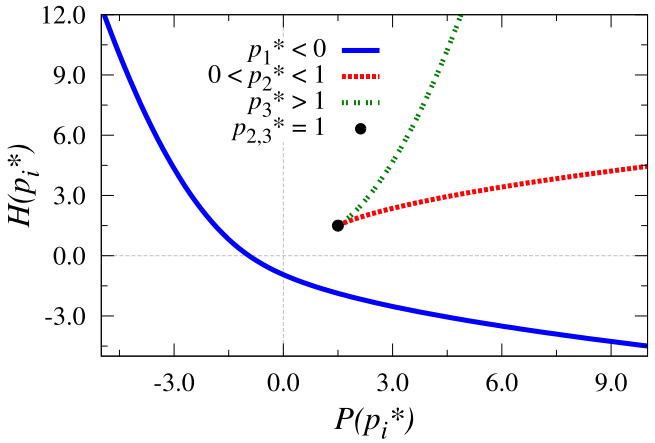

FIG. 2. Curves on the (P, H) plane for Eq. (17).

for real time, describing motion on the separatrix of the hyperbolic fixed point. On the contrary, if $p^* < 0$ or if $p^* > 1$, Eq. (18) has no real-valued solution as the associated fixed point is elliptic.

B. Phase portrait analysis for $N = M = 1$

The phase portrait of the system in the (p, y) variables is shown in Fig. 3 and has special boundaries. Indeed, variable $y = x - \theta$ is 2π-periodic and the wave intensity must be positive so that $p \le P$, and the portrait will be plotted over half a cylinder.

As already seen in Sec. III A, the fixed point at $y_1^* = 0$ has elliptic stability for all values of total momentum P so that the system dynamics around the elliptic point is represented by closed trajectories.

The black line in the phase portraits represents the trajectory for which the wave intensity I passes through 0. The ordinate P for p does not correspond to a continuum of values for y, because Eq. (10a) is meaningless if $\cos y \neq 0$. Thus, only abscissae $y = \pm\pi/2$ are permitted when $I = 0$, and then the wave phase is actually undefined. But the dynamics is well defined in Cartesian variables (X, Y) and, if the wave turns out to vanish at a time, then $\dot{X}^2 + \dot{Y}^2 = 1$ implies that I cannot remain zero, i.e., the potential acting on the particle cannot remain flat. Actually, as the particle position is a smooth function of time, what occurs when I vanishes is that the wave phase jumps between $x - \pi/2$ and $x + \pi/2$, and the trajectory in (p, y) variables transits through this connection with $\dot{p} = 0$ and $\ddot{p} = -1$ so that the value $p = P$ is a non-degenerate local maximum of p along the trajectory. According to (9), this trajectory has energy $H = P^2/2$. The phase jump by π instantly interchanges the locations of the wave potential's trough and crest, which is a very efficient mechanism generating chaos and violent mixing in the system with more than one particle.[37]

For $P < 3/2$, the black line separates the cylinder into two domains: the orbits rotating (clockwise) around the elliptic fixed point and the orbits winding (toward the left) around the cylinder. For the value $P = 3/2$, the system has a saddle-center bifurcation

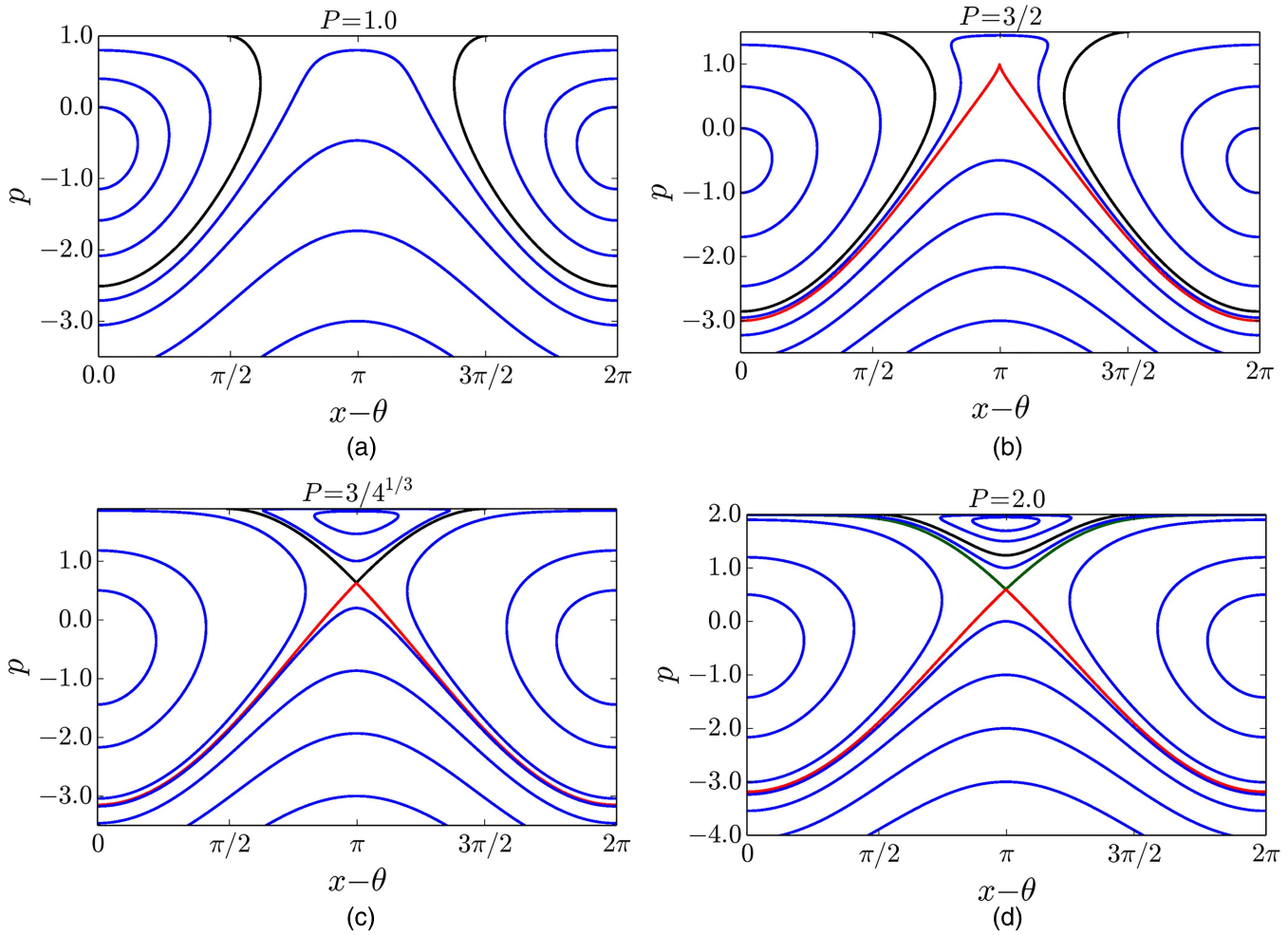

FIG. 3. Phase portrait with $N = 1$ for the single wave Hamiltonian (9). Panel (a) shows the case $P < 3/2$ (before bifurcation), panel (b) shows the case $P = 3/2$ (at the saddle-center bifurcation), panel (c) corresponds to total momentum $P = 3/4^{1/3}$, for which the trajectory containing $I = 0$ coincides with the upper branch of the X point separatrix, and panel (d) shows the dynamics after the global bifurcation.

at which an elliptic–hyperbolic pair coalesce, as shown by the black point in the bifurcation diagram (Figs. 1 and 2). The trajectory asymptotic to the bifurcation point is represented by the red line in Fig. 3(b).

For $P > 3/2$, we see two different types of stability at the same fixed point coordinate $y^*_{2,3} = \pi$. The upper fixed point is elliptic, circled by orbits rotating counterclockwise in the phase portrait. The lower fixed point is hyperbolic, and the lower branch of its separatrix winds (to the left) around the cylinder: from $t \to -\infty$, the particle leaves the crest of the wave potential, it passes at the bottom of the wave potential when the wave has its largest amplitude, and it asymptotes again the next crest of the potential for $t \to +\infty$ so that $\int_{-\infty}^{+\infty} \dot{y}(t)\, dt = -2\pi$. The upper branch of the separatrix is, for $3/2 < P < 3/4^{1/3}$, a counterclockwise loop around the elliptic fixed point, with $\cos(x - \theta)$ always negative: from $t \to -\infty$, the particle leaves the crest of the wave potential, it passes again at the same crest of the wave potential when the wave has its smallest amplitude, and it asymptotes again the same crest of the potential for $t \to +\infty$ so that $\int_{-\infty}^{+\infty} \dot{y}(t)\, dt = 0$.

Figure 3(c) shows another special value of P for which the phase portrait changes: when $P = 3/4^{1/3}$, the points of null wave intensity belong to the separatrix of the X point ($y^*_2 = \pi$, $p^*_2\sqrt{2(P - p^*_2)} = 1$). The trajectory for which this happens has energy $H_{I=0} = P^2/2$ (for passing through $I = 0$) and this energy must also be equal to the energy of the X point, i.e., $H_{I=0} = (p^*_2)^2/2 + \sqrt{2(P - p^*_2)}$ (where p^*_2 is the X point momentum obtained by solving condition $p^*_2\sqrt{2(P - p^*_2)} = 1$). Thus, $P^2 = (p^*_2)^2 + 2\sqrt{2(P - p^*_2)} = (p^*_2)^2 + 2/p^*_2$, and the X point condition implies that $P = p^*_2 + 1/(2(p^*_2)^2)$ so that $(p^*_2)^2 + 1/p^*_2 + 1/(4(p^*_2)^4) = (p^*_2)^2 + 2/p^*_2$, i.e., $p^*_2 = 4^{-1/3}$ and $P = 3/4^{1/3}$. Because this phase portrait connects

two distinct points (the $I = 0$ point and the X point), the system undergoes a global bifurcation at $P = 3/4^{1/3}$.

For $P > 3/4^{1/3}$, the upper branch of the separatrix winds around the cylinder (to the right): from $t \to -\infty$, the particle leaves the crest of the wave potential, it passes at the bottom of the wave potential when the wave has its smallest amplitude, and it asymptotes the next crest of the potential for $t \to +\infty$ so that $\int_{-\infty}^{+\infty} \dot{y}(t)\, \mathrm{d}t = 2\pi$. Moreover, for $P > 3/4^{1/3}$, the black line containing the points with $I = 0$ separates two domains: above it, trajectories circle counterclockwise around the elliptic fixed point at $y_3^* = \pi$, whereas trajectories wind around the cylinder (to the right) between it and the upper branch of the separatrix.

The system with $N = 1$ particle coupled to $M = 1$ wave does not generate chaos. In Sec. IV, we describe the emergence of chaos by increasing the number of particles to $N = 2$ in the single wave model. The symmetric case with $N = 1$, $M = 2$, although departing from the SWM, can be described by the same Hamiltonian (1) and (2), and chaos occurs as soon as two waves with different phase velocities are present.[1]

IV. THE SINGLE WAVE AND TWO PARTICLES

A. General aspects

The $M = 1$, $N = 2$ system is the first step toward the dynamics of the paradigmatic single wave model, where the case of many particles sheds much light on fundamental plasma instabilities, in particular, the bump-on-tail. The reference Hamiltonian $H_{\mathrm{sc}}^{2,1}$ (from now on, denoted simply H)

$$H = \frac{p_1^2}{2} + \frac{p_2^2}{2} + \omega_0 \frac{X^2 + Y^2}{2} + \varepsilon Y(\sin x_1 + \sin x_2) - \varepsilon X(\cos x_1 + \cos x_2) \tag{19a}$$

$$= \frac{p_1^2}{2} + \frac{p_2^2}{2} + \omega_0 I - \varepsilon\sqrt{2I}(\cos(x_1 - \theta) + \cos(x_2 - \theta)) \tag{19b}$$

describes two particles interacting self-consistently with one wave. Again, a Galileo transformation enables us to set $\omega_0 = 0$, leaving

$$H = \frac{p_1^2}{2} + \frac{p_2^2}{2} + \varepsilon(Y(\sin x_1 + \sin x_2) - X(\cos x_1 + \cos x_2)) \tag{20a}$$

$$= \frac{p_1^2}{2} + \frac{p_2^2}{2} - \varepsilon\sqrt{2I}(\cos(x_1 - \theta) + \cos(x_2 - \theta)). \tag{20b}$$

Finally, rescaling all variables as $t' = \lambda^{-1}t$, $x' = x$, $\theta' = \theta$, $p' = \lambda p$, $I' = \lambda I$, $P' = \lambda P$, $X' = \lambda^{1/2}X$, $Y' = \lambda^{1/2}Y$, and $H' = \lambda^2 H$ shows that the coupling parameter can also be scaled away with $\varepsilon' = \lambda^{3/2}\varepsilon$. Thus, we are left with three cases:

1. $\varepsilon = 0$: the system is uncoupled;
2. $\varepsilon = 1$: the coupling has unit strength and favors $x_{1,2} \sim \theta$ energetically; and
3. $\varepsilon = -1$: the coupling has unit strength and favors $x_{1,2} \sim \pi + \theta$ energetically, but this can be absorbed in the change of variable $\theta' = \theta + \pi$.

The model is thus completely parametrized by total energy H and total momentum $P = p_1 + p_2 + (X^2 + Y^2)/2$ for $\varepsilon = 1$. From here on, we set $\varepsilon = 1$. A similar Hamiltonian was considered by del Castillo-Negrete and Firpo,[37,43] with a different wave–particle coupling. Our results complement theirs.

For the $M = N = 1$ model, the fact that the wave intensity must be positive implied that the particle momentum p was bounded from above by P. With two particles, total momentum P sets no bound on a single particle momentum since only $p_1 + p_2$ is bounded by P.

The original dynamics (19a) or (20a) has three degrees of freedom, with phase space $(\mathbb{T} \times \mathbb{R})^2 \times \mathbb{R}^2$, where particles evolve on the cylinder $\mathbb{T} \times \mathbb{R}$ and the harmonic oscillator (*viz.*, the wave) evolves in the plane $\mathbb{R}^2$. Given the two conserved quantities, the dynamics is restricted to four-dimensional manifolds, and the motions generate Poincaré maps in three-dimensional sections.

The equations of motion read

$$\dot{x}_r = p_r, \tag{21a}$$

$$\dot{p}_r = -X\sin x_r - Y\cos x_r = -\sqrt{2I}\sin(x_r - \theta), \tag{21b}$$

$$\dot{X} = \sin x_1 + \sin x_2, \tag{21c}$$

$$\dot{Y} = \cos x_1 + \cos x_2, \tag{21d}$$

$$\dot{\theta} = -(2I)^{-1/2}(\cos(x_1 - \theta) + \cos(x_2 - \theta)), \tag{21e}$$

$$\dot{I} = \sqrt{2I}(\sin(x_1 - \theta) + \sin(x_2 - \theta)). \tag{21f}$$

For $\omega_0 > 0$, Hamiltonian (19b) is bounded from below: $|\cos(x_1 - \theta) + \cos(x_2 - \theta)| \le 2$ so that

$$H \ge \frac{p_1^2 + p_2^2}{2} - 2\sqrt{2I} + \omega_0 I, = \frac{p_1^2 + p_2^2}{2} + \frac{\omega_0}{2}\left(\sqrt{2I} - \frac{2}{\omega_0}\right)^2 - \frac{2}{\omega_0}. \tag{22}$$

For $\omega_0 \le 0$, Hamiltonian (19b) is not bounded from below: one may have $x_1 = x_2 = \theta$, $p_1 = p_2 = 0$ and I arbitrarily large. Then, $H = \omega_0 I - 2\sqrt{2I} \to -\infty$ as $I \to \infty$. However, for fixed P, the Hamiltonian is bounded from below even for $\omega_0 \le 0$,

$$\begin{aligned} H &\ge \frac{p_1^2 + p_2^2}{2} - 2\sqrt{2I} + \omega_0 I \\ &= \frac{(p_1 + p_2)^2 + (p_1 - p_2)^2}{4} - 2\sqrt{2}\sqrt{P - (p_1 + p_2)} + \omega_0(P - (p_1 + p_2)) \\ &\ge \frac{(p_1 + p_2)^2}{4} - 2\sqrt{2}\sqrt{P - (p_1 + p_2)} + \omega_0(P - (p_1 + p_2)), \end{aligned} \tag{23}$$

and the last two terms cannot diverge faster than the first one if P is bounded.

Given P and H, Eq. (23) implies that p_1 and p_2 are bounded, and Eq. (22) shows that I is bounded too. Since x_1, x_2, and θ vary on the unit circle, the constant (P, H) manifolds are compact.

This discussion about boundedness shows how important the conservation of momentum is. Moreover, it stresses how the notion of energy depends on the observer's viewpoint: a mere Galileo transformation changes the model from H bounded from below for any P (with $\omega_0 > 0$) to H bounded from below conditionally on a fixed P.

B. Reduction to 2 degrees of freedom

The intersection of energy and momentum surfaces is compact for every (H, P), for any fixed ω_0. Indeed, the generalized coordinates (x_1, x_2, θ) range over a 3-torus. The generalized momenta must satisfy the above inequalities implying that neither p_1 nor p_2 can diverge, and hence $I = P - p_1 - p_2$ cannot diverge either.

For a fixed P, consider the reduced dynamics in terms of (y_1, y_2, p_1, p_2), with $I = P - p_1 - p_2$ and $y_r = x_r - \theta$. Then,

$$\dot{y}_r = p_r + \frac{\cos y_1 + \cos y_2}{\sqrt{2(P - p_1 - p_2)}}, \tag{24a}$$

$$\dot{p}_r = -\sqrt{2(P - p_1 - p_2)}\,\sin y_r, \tag{24b}$$

with the conserved Hamiltonian

$$H = \frac{p_1^2}{2} + \frac{p_2^2}{2} - \sqrt{2(P - p_1 - p_2)}(\cos y_1 + \cos y_2). \tag{25}$$

As the $N = 1$ case is recovered by setting $y_1 = y_2$ and $p_1 = p_2$ and rescaling time, energy, and coupling constant, let $\sigma = P/2$. With variables $z_1 = (y_1 + y_2)/2$, $z_2 = (y_1 - y_2)/2$, $w_1 = (p_1 + p_2)/2$, and $w_2 = (p_1 - p_2)/2$, the Poisson brackets are

$$\begin{aligned}[f,g] &= \partial_{p_1} f\,\partial_{y_1} g - \partial_{y_1} f\,\partial_{p_1} g + \partial_{p_2} f\,\partial_{y_2} g - \partial_{y_2} f\,\partial_{p_2} g \\ &= \frac{1}{2}(\partial_{w_1} f\,\partial_{z_1} g - \partial_{z_1} f\,\partial_{w_1} g \\ &\quad + \partial_{w_2} f\,\partial_{z_2} g - \partial_{z_2} f\,\partial_{w_2} g)\end{aligned} \tag{26}$$

so that Hamilton's canonical evolution equations read

$$\begin{aligned}\dot{g} = [H, g] &= \left(\partial_{w_1}\frac{H}{2}\right)\partial_{z_1} g - \left(\partial_{z_1}\frac{H}{2}\right)\partial_{w_1} g \\ &\quad + \left(\partial_{w_2}\frac{H}{2}\right)\partial_{z_2} g - \left(\partial_{z_2}\frac{H}{2}\right)\partial_{w_2} g.\end{aligned} \tag{27}$$

Specifically,

$$\begin{aligned}\dot{z}_1 &= w_1 + \frac{\cos(z_1 + z_2) + \cos(z_1 - z_2)}{\sqrt{4(\sigma - w_1)}} \\ &= w_1 + \frac{\cos z_1 \cos z_2}{\sqrt{\sigma - w_1}},\end{aligned} \tag{28a}$$

$$\dot{z}_2 = w_2, \tag{28b}$$

$$\begin{aligned}\dot{w}_1 &= -\sqrt{4(\sigma - w_1)}\,\frac{\sin(z_1 + z_2) + \sin(z_1 - z_2)}{2} \\ &= -2\sqrt{\sigma - w_1}\,\sin z_1 \cos z_2,\end{aligned} \tag{28c}$$

$$\begin{aligned}\dot{w}_2 &= -\sqrt{4(\sigma - w_1)}\,\frac{\sin(z_1 + z_2) - \sin(z_1 - z_2)}{2} \\ &= -2\sqrt{\sigma - w_1}\,\cos z_1 \sin z_2.\end{aligned} \tag{28d}$$

The new variables (w_1, w_2, z_1, z_2) are not canonically equivalent to the original ones (since the bracket undergoes a rescaling by $1/2$) but the quantity

$$\begin{aligned}E = H/2 &= \frac{w_1^2}{2} + \frac{w_2^2}{2} - \sqrt{\sigma - w_1}\,(\cos(z_1 + z_2) + \cos(z_1 - z_2)) \\ &= \frac{w_1^2}{2} + \frac{w_2^2}{2} - 2\sqrt{\sigma - w_1}\,\cos z_1 \cos z_2\end{aligned} \tag{29}$$

plays the role of a Hamiltonian in these new variables as the action differential of the system may be written as

$$\begin{aligned}\mathrm{d}S &= \sum_r p_r\,\mathrm{d}x_r + I\,\mathrm{d}\theta - H\,\mathrm{d}t \\ &= \sum_r p_r\,\mathrm{d}y_r + P\,\mathrm{d}\theta - H\,\mathrm{d}t \\ &= 2\left(\sum w_r\,\mathrm{d}z_r + \sigma\,\mathrm{d}\theta - E\,\mathrm{d}t\right).\end{aligned} \tag{30}$$

Note that $E = H/2$ is also the energy per particle, like $\sigma = P/2$ is the momentum per particle.

Energy E can be rewritten in the form

$$E = E_1(w_1, z_1) + E_2(w_2, z_2, w_1, z_1), \tag{31}$$

with

$$E_1 = \frac{w_1^2}{2} - 2\sqrt{\sigma - w_1}\,\cos z_1, \tag{32}$$

$$E_2 = \frac{w_2^2}{2} + 2\sqrt{\sigma - w_1}\,\cos z_1(1 - \cos z_2). \tag{33}$$

This form extracts for (w_1, z_1) an effective Hamiltonian E_1, which is the $N = 1$ model, up to rescaling the coupling coefficient with a factor $\sqrt{2}$. The second term E_2 is positive if $\cos z_1 > 0$, which corresponds to the case where the two particles are not "too far" from each other, and describes their relative motion as that of a pendulum with time-dependent parameters.

The periodic boundary conditions $y_r \equiv y_r + 2\pi \mod (2\pi)$ imply that the configuration space is a torus. The covering of this torus with cells of the form $z_r \equiv z_r + 2\pi \mod (A_r)$ for an appropriate A_r is not consistent if one sets $A_1 = A_2 = \pi$ for both z_1 and z_2. For the sake of safety, we set $A_1 = A_2 = 2\pi$, which implies that the new cells have an area equal to twice that of the original ones, and two points in the cell (z_1, z_2) correspond to a single point in (y_1, y_2).

We analyze Poincaré sections at $z_2 \equiv 0 \mod (2\pi)$. For a given σ, a point (w_1, z_1) in this section may correspond to different energies E, depending on w_2. More precisely, when both particles have the same $(p, y) = (p_1, y_1) = (p_2, y_2)$, we have the $N = 1$ dynamics, with just a doubled mass and doubled coupling constant. This generates a family of solutions to the $N = 2$ case. However, for $N = 2$ with $z_2 = 0$ and an arbitrary w_2, the two-particle case always has more energy than the $N = 1$ case. Since E is conserved, the initial

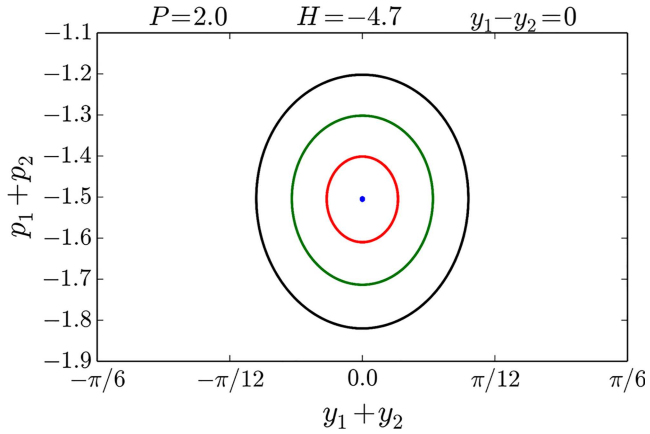

FIG. 4. Interception of trajectories with the Poincaré section located at $y_1 - y_2 = 0$. This panel represents the dynamics in the neighborhood of the elliptic fixed point at $y_1 - y_2 = 0$ with total energy $H = -4.7$.

excess energy $E_2 = w_2^2/2$ in the two-particle system may be taken as a perturbation parameter enabling chaos near the orbits of the integrable system.

The $(z_2 = 0, w_2 = 0)$ trajectory appears in the Poincaré section $z_2 = 0$ as the boundary of the domain accessible for a given total energy H. Its stability is governed by the linearized equations

$$\dot{z}_1 = w_1 + \frac{\cos z_1}{\sqrt{\sigma - w_1}}, \tag{34a}$$

$$\dot{w}_1 = -2\sqrt{\sigma - w_1}\,\sin z_1, \tag{34b}$$

$$\delta\dot{z}_2 = \delta w_2, \tag{34c}$$

$$\delta\dot{w}_2 = -(2\sqrt{\sigma - w_1}\,\cos z_1)\delta z_2, \tag{34d}$$

where the (w_1, z_1) dynamics is the master and the (w_2, z_2) dynamics is the slave. Indeed, the Taylor expansion $\cos \delta z_2 = 1 - (\delta z_2)^2/2 + \cdots$ implies that δz_2 cannot appear in the (w_1, z_1) dynamics. This master–slave description is, for $(\delta w_2, \delta z_2)$, a linearized version of Boozer's analysis of the emergence of chaos in Hamiltonian systems.[45]

If the (w_1, z_1) trajectory remains confined in the band $\cos z_1 > 0$ (or $-\pi/2 < z_1 < \pi/2$), then the small perturbation $(\delta z_2, \delta w_2)$ obeys a linear evolution equation with time-periodic coefficients of Hill type, $\delta\ddot{z}_2 = -g(t)\delta z_2$ with a positive function $g(t)$. Though there may be resonances for some such (w_1, z_1) trajectories, the perturbation may remain bounded. Indeed, the Poincaré sections show nice KAM (Kolmogorov-Arnold-Moser) tori in this range (Fig. 4) and one checks that E_2 is positive definite for $\cos z_1 > 0$.

In contrast, when the (w_1, z_1) trajectory enters the band $\cos z_1 < 0$ (or $-\pi/2 < z_1 - \pi < \pi/2$), then the perturbation obeys $\delta\ddot{z}_2 = -g(t)\delta z_2$ with a negative function $g(t)$. During this time, the perturbation is amplified (and the more as z_1 approaches π), and the system may leave the linear regime. Then, $\cos z_2$ is no longer close to 1 and the relative motion (w_2, z_2) feeds back upon the "master" variables. Such a process easily generates chaos, and one may expect that, soon enough, the trajectory approaches $z_1 \approx \pi$ and the associated hyperbolic point. As a result, one may expect a well-developed chaotic behavior for trajectories entering the band $\cos z_1 < 0$. Energetically, E_2 has an indefinite signature for $\cos z_1 < 0$.

The (w_1, z_1) trajectories which come close to $w_1 = \sigma$ are also likely to behave chaotically, because this line corresponds to $I = 0$, and on this line, the angle z_1 spontaneously jumps by π to account for the sign reversal of both X and Y when the wave crosses null-amplitude. Then, the corner of the wave cat's eye in original variables (x_r, p_r) suddenly becomes its center and, conversely, which is a very efficient mixing process.[37,46]

V. FIXED POINTS AND SPECIAL TRAJECTORIES

The equilibrium solutions for the case with $N = 2$ are given in terms of (x_1, x_2, p_1, p_2) such that (I, θ) remain constant. Thus, if $I > 0$ the amplitude and the phase remain constant only if $x_2 = \pi + x_1 \bmod (2\pi)$, which implies $p_1 = p_2$. The latter requires $\sin(x_1 - \theta) = \sin(x_2 - \theta)$, which must, therefore, vanish so that $x_1 = \theta \bmod \pi$ and $p_1 = p_2 = 0$. Then, $P = I$ and $H = 0$. One particle stands on the unstable fixed point of the wave $(\pi + \theta)$, while the other particle is at the bottom of the potential well (θ). It has actually been proved that, for a finite-amplitude wave with fixed (I, θ), particles cannot move with respect to the wave, whatever their number N.[47]

For $I = 0$, i.e., $X = Y = 0$, the amplitude remains 0 only if $x_1 = \pi + x_2 \bmod (2\pi)$, implying $p_1 = p_2$ (which must not vanish) and then $P = 2p_1$ and $H = P^2/4$. Both particles move at the same velocity and form a (two-particle) ballistic beam. Such solutions exist for any number $N \geq 2$ particles.[48]

The limit case $I = 0$ (for which θ is undefined) in the first type is also the special case $P = 0$ in the second type. Moreover, if we seek regular solutions with merely a constant phase, say, $\theta = 0$ with no loss of generality, this imposes $Y = 0$ and $\dot{Y} = 0$; hence, $x_2 = \pi \pm x_1$, which has two solutions:

1. $x_2 = \pi + x_1$ implies $\dot{X} = 0$, which was considered above: X itself must be 0.
2. $x_2 = \pi - x_1$ implies $p_2 = -p_1$, but it also implies $\sin x_1 = \sin x_2$ so that $\dot{X} = 2 \sin x_1$. However, total momentum $P = X^2/2$ must remain constant, which implies $\sin x_1 = 0$; hence, $x_1 = 0$ and $x_2 = \pi$ (or the opposite).

Thus, any other solution must have a time-dependent phase.

A. Vanishing wave

For a vanishing wave amplitude, the special solution has its two particles moving at a finite velocity $v = p_1 = p_2 = P/2$. Then, let $x_1 = vt$ and $x_2 = \pi + vt$ (by a proper choice of the origin of time

if $\nu \neq 0$). The resulting linearized dynamics reads

$$\frac{\mathrm{d}}{\mathrm{d}t}\begin{pmatrix}\delta x_1\\ \delta p_1\\ \delta x_2\\ \delta p_2\\ \delta X\\ \delta Y\end{pmatrix} = \begin{pmatrix} 0 & 1 & 0 & 0 & 0 & 0\\ 0 & 0 & 0 & 0 & -\sin \nu t & -\cos \nu t\\ 0 & 0 & 0 & 1 & 0 & 0\\ 0 & 0 & 0 & 0 & \sin \nu t & \cos \nu t\\ \cos \nu t & 0 & -\cos \nu t & 0 & 0 & 0\\ -\sin \nu t & 0 & \sin \nu t & 0 & 0 & 0 \end{pmatrix} \times \begin{pmatrix}\delta x_1\\ \delta p_1\\ \delta x_2\\ \delta p_2\\ \delta X\\ \delta Y\end{pmatrix}. \tag{35}$$

The explicit dependence of the matrix elements on time makes this linear dynamics a Floquet system.[48]

One easily eliminates one pair of variables by introducing

$$s_1 = (\delta x_1 + \delta x_2)/2, \tag{36a}$$

$$u_1 = \delta p_1 + \delta p_2, \tag{36b}$$

$$s_2 = \delta x_1 - \delta x_2, \tag{36c}$$

$$u_2 = (\delta p_1 - \delta p_2)/2 \tag{36d}$$

so that the system decouples to

$$\frac{\mathrm{d}}{\mathrm{d}t}\begin{pmatrix}s_1\\ u_1\end{pmatrix} = \begin{pmatrix}0 & 1/2\\ 0 & 0\end{pmatrix}\begin{pmatrix}s_1\\ u_1\end{pmatrix}, \tag{37}$$

along with

$$\frac{\mathrm{d}}{\mathrm{d}t}\begin{pmatrix}s_2\\ u_2\\ \delta X\\ \delta Y\end{pmatrix} = \begin{pmatrix} 0 & 2 & 0 & 0\\ 0 & 0 & -\sin \nu t & -\cos \nu t\\ \cos \nu t & 0 & 0 & 0\\ -\sin \nu t & 0 & 0 & 0 \end{pmatrix}\begin{pmatrix}s_2\\ u_2\\ \delta X\\ \delta Y\end{pmatrix}. \tag{38}$$

Total momentum reads, to first order, $\delta P = u_1$, and energy to second order

$$\delta^2 H = \frac{u_1^2}{4} + u_2^2 + (\delta X)s_2 \sin \nu t + (\delta Y)s_2 \cos \nu t, \tag{39}$$

and the decoupling ensures that u_1 remains constant. Note that the perturbative approach does not require momentum conservation to second order, as the dynamics is linearized. The second order energy is relevant because the Hamiltonian is derived with respect to the perturbations to generate the dynamics.

Though the decoupling reduces the number of dynamical variables in (38), conservation laws no longer simplify the dynamics: total momentum conservation places no constraint on this system, and total energy is now formally time-dependent. However, since the coefficients in (38) are trigonometric functions of time, one may view this system like forcing the wave oscillator by the particles reference motion, at the Doppler-shifted angular frequency ν.

It is thus interesting to perform a Galileo transformation to the beam frame, introducing variables $x'_r = x_r - \nu t$, $p'_r = p_r - \nu$, $X' + \mathrm{i}Y' = (X + \mathrm{i}Y)\,\mathrm{e}^{\mathrm{i}\nu t}$ so that (21a), (21b), (21c), and (21d) read

$$\dot{x}'_r = p'_r, \tag{40a}$$

$$\dot{p}'_r = -X' \sin x'_r - Y' \cos x'_r, \tag{40b}$$

$$\dot{X}' = \sin x'_1 + \sin x'_2 - \nu Y', \tag{40c}$$

$$\dot{Y}' = \cos x'_1 + \cos x'_2 + \nu X'. \tag{40d}$$

The null solution now reads $x'_1 = 0$, $x'_2 = \pi$, $p'_1 = p'_2 = 0$, and $X' = Y' = 0$, and the linearized dynamics is now autonomous,

$$\frac{\mathrm{d}}{\mathrm{d}t}\begin{pmatrix}\delta x'_1\\ \delta p'_1\\ \delta x'_2\\ \delta p'_2\\ \delta X'\\ \delta Y'\end{pmatrix} = \begin{pmatrix} 0 & 1 & 0 & 0 & 0 & 0\\ 0 & 0 & 0 & 0 & 0 & -1\\ 0 & 0 & 0 & 1 & 0 & 0\\ 0 & 0 & 0 & 0 & 0 & 1\\ 1 & 0 & -1 & 0 & 0 & -\nu\\ 0 & 0 & 0 & 0 & \nu & 0 \end{pmatrix}\begin{pmatrix}\delta x'_1\\ \delta p'_1\\ \delta x'_2\\ \delta p'_2\\ \delta X'\\ \delta Y'\end{pmatrix}. \tag{41}$$

Again, introducing s_1, s_2, u_1, and u_2 decouples the system, and the nontrivial part reads

$$\frac{\mathrm{d}}{\mathrm{d}t}\begin{pmatrix}s_2\\ u_2\\ \delta X'\\ \delta Y'\end{pmatrix} = \begin{pmatrix} 0 & 2 & 0 & 0\\ 0 & 0 & 0 & -1\\ 1 & 0 & 0 & -\nu\\ 0 & 0 & \nu & 0 \end{pmatrix}\begin{pmatrix}s_2\\ u_2\\ \delta X'\\ \delta Y'\end{pmatrix}. \tag{42}$$

The characteristic polynomial of the matrix in the right-hand side of (41) is

$$P_4(\lambda) = \lambda^4 + \nu^2\lambda^2 + 2\nu, \tag{43}$$

which admits four roots

$$\lambda = \pm\frac{\mathrm{i}}{\sqrt{2}}\sqrt{\nu^2 \pm \sqrt{\nu^4 - 8\nu}}. \tag{44}$$

If $\nu < 0$, viz., if the particles are slower than the wave, this defines two real roots and two imaginary roots: the reference solution is unstable. If $0 < \nu < 2$, viz., if the particles are moderately faster than the wave, this defines a quartet of complex roots $\pm\alpha \pm \mathrm{i}\beta$: the reference solution is also unstable. If $\nu > 2$, viz., if the particles are significantly faster than the wave, all four roots are purely imaginary: the reference state is stable.

At $\nu = 0$, the case coincides with the zero-amplitude limit of the other class of solutions. For ν close to 0 and negative, the eigenvalues have modulus $(-2\nu)^{1/4}$ and lie on the real and imaginary axes. For ν close to 0 and positive, the eigenvalues have modulus $(2\nu)^{1/4}$ and lie on the bissectrices. At $\nu = 2$, the model exhibits a Kreĭn collision (or Hamiltonian Hopf bifurcation).[49]

B. Coinciding particles

If the two particles are at the same position with the same velocity at $t = 0$, they will never separate. Indeed, with variables (p_r, x_r, Y, X), the evolution equations (21a), (21b), (21c) and (21d) are smooth and have unique solutions globally in time.

For $z_2 = 0$ and $w_2 = 0$, the evolution equations (34a) and (34b) with time t can be rewritten as (10a) and (10b) with a time

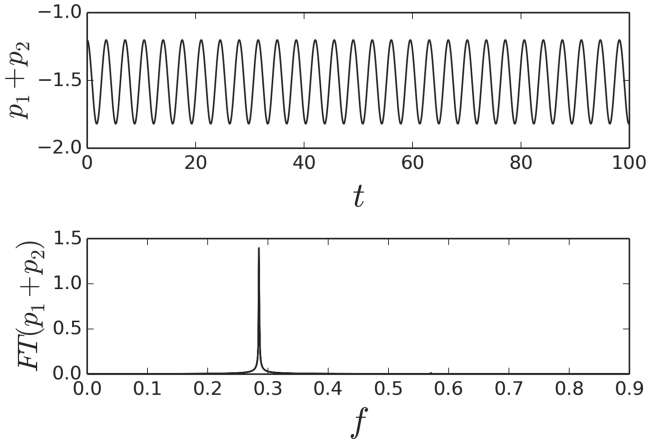

FIG. 5. Time evolution and Fourier transform of the particles total momentum for the black (outer oval) trajectory in Fig. 4.

s by rescaling $s = 2^{1/3}t$, $y = z_1$, $p = 2^{-1/3}w_1$, $P_{N=1} = 2^{-1/3}\sigma$, and $H_{N=1} = 2^{-2/3}H_{N=2}$. Note that the rescaling of time implies that frequencies and Lyapunov exponents rescale accordingly.

The wave amplitude $I > 0$ implies that $p_1 + p_2 < P$, then θ is well defined, and we have $\sin y_1 = \sin y_2 = 0$. So when both particles are in the same position $y_1 = y_2 = 0$, from (24), one finds

$$p_1 = p_2 = \frac{-1}{\sqrt{\sigma - p_1}} < 0. \tag{45}$$

The linear stability analysis from Eq. (24),

$$\delta\dot{y}_1 = \delta p_1, \tag{46a}$$

$$\delta\dot{p}_1 = \frac{2}{p_1}\delta y_1, \tag{46b}$$

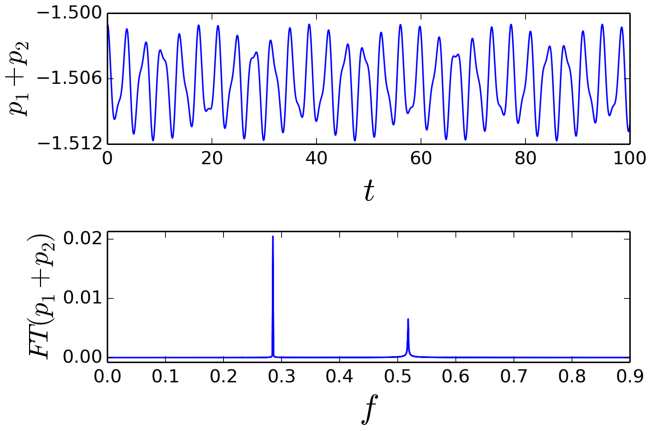

FIG. 6. Time evolution and Fourier transform of the particles total momentum for the blue (central point) trajectory in Fig. 4.

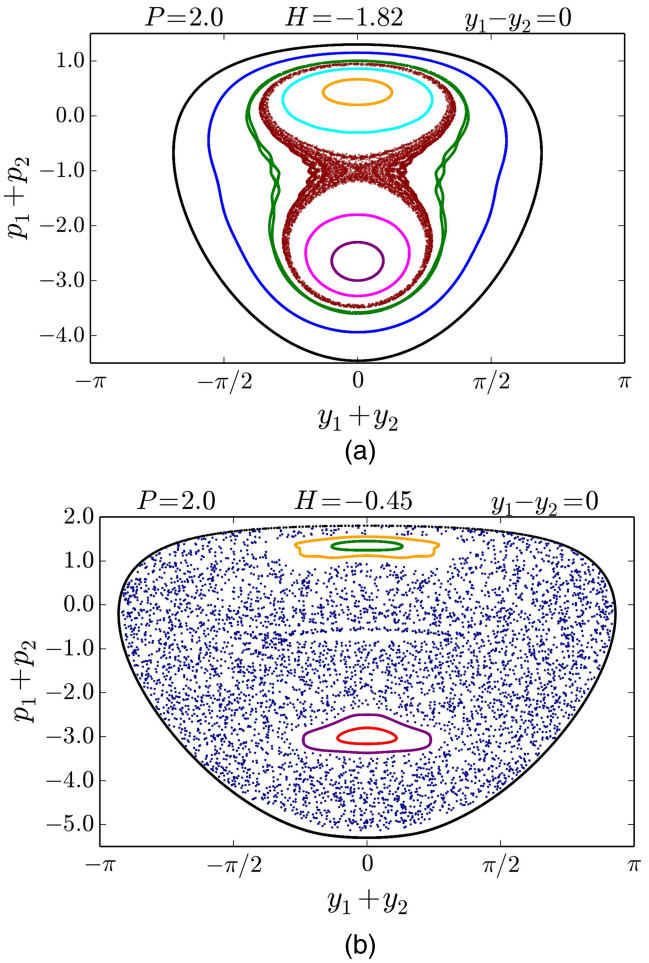

FIG. 7. Interception of trajectories with the Poincaré section located at $y_1 - y_2 = 0$ for negative H values. The panels represent the dynamics in the neighborhood of the elliptic fixed point at $y_1 - y_2 = 0$ with total energy (a) $H = -1.82$ and (b) $H = -0.45$.

$$\delta\dot{y}_2 = \delta p_2, \tag{46c}$$

$$\delta\dot{p}_2 = \frac{2}{p_1}\delta y_2, \tag{46d}$$

shows that this case is stable so that both particles oscillate at the same frequency near the bottom of the wave potential well. As we see in Figs. 4–6, at low energy, the system undergoes harmonic oscillations near the fixed point at $y_1 = y_2 = 0$. For increasing energy, the nonlinear coupling generates chaos near this 1:1 resonance.

Now, considering the case where both particles coincide at the same position $y_1 = y_2 = \pi$ (unstable position of the potential),

$$p_1 = p_2 = \frac{1}{\sqrt{\sigma - p_1}} > 0, \tag{47}$$

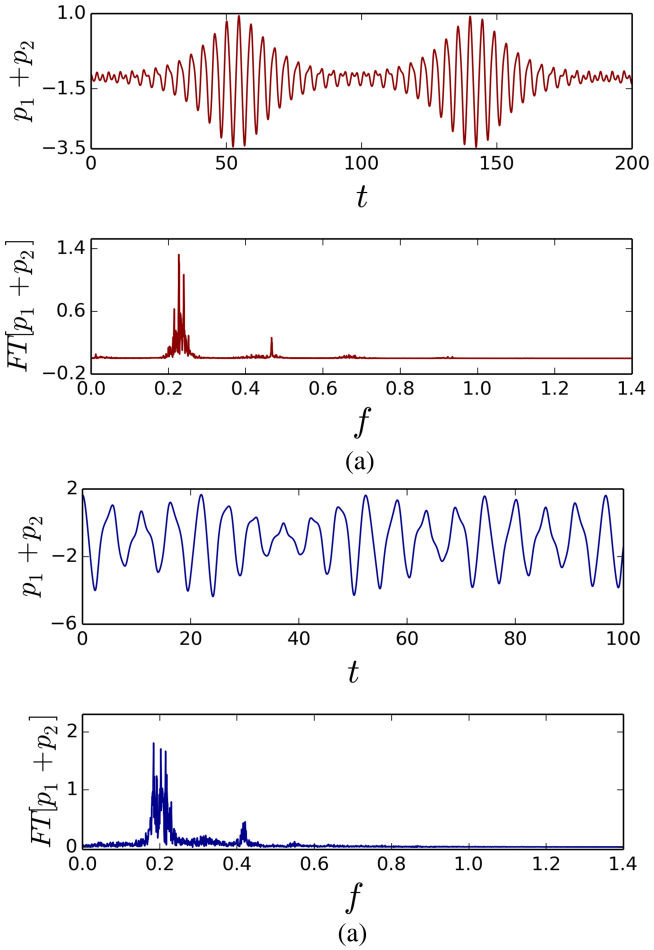

FIG. 8. Time evolution and Fourier transform of the particles total momentum for (a) the dark red (similar to an "8") trajectory in Fig. 7(a) and (b) the blue (chaotic) trajectory in Fig. 7(b).

and this solution exists only if $\sigma \geq 3/4^{1/3}$. Here, we have two possibilities, namely, $p_1 = p_2 = p^*_{\text{low}}$ and $p_1 = p_2 = p^*_{\text{high}}$.

The linearized equations read

$$\delta\dot{p}_r = 2\sqrt{\sigma - p^*}\,\delta\dot{y}_r, \tag{48a}$$

$$\delta\dot{y}_r = \delta p_r - \frac{1}{4(\sigma - p^*)^{3/2}}(\delta p_1 - \delta p_2), \tag{48b}$$

or

$$\begin{pmatrix} \delta\dot{y}_1 \\ \delta\dot{y}_2 \\ \delta\dot{p}_1 \\ \delta\dot{p}_2 \end{pmatrix} = \begin{pmatrix} 0 & 0 & 1-K & -K \\ 0 & 0 & -K & 1-K \\ 2\sqrt{\sigma - p^*} & 0 & 0 & 0 \\ 0 & 2\sqrt{\sigma - p^*} & 0 & 0 \end{pmatrix} \begin{pmatrix} \delta y_1 \\ \delta y_2 \\ \delta p_1 \\ \delta p_2 \end{pmatrix}, \tag{49}$$

with

$$K = \frac{1}{4(\sigma - p^*)^{3/2}} = p^{*3}/4. \tag{50}$$

Thus,

$$\begin{pmatrix} \delta\dot{z}_2 \\ \delta\dot{z}_1 \\ \delta\dot{w}_2 \\ \delta\dot{w}_1 \end{pmatrix} = \begin{pmatrix} 0 & 0 & 1 & 0 \\ 0 & 0 & 0 & 1-2K \\ 2\sqrt{\sigma - p^*} & 0 & 0 & 0 \\ 0 & 2\sqrt{\sigma - p^*} & 0 & 0 \end{pmatrix} \begin{pmatrix} \delta z_2 \\ \delta z_1 \\ \delta w_2 \\ \delta w_1 \end{pmatrix}, \tag{51}$$

and the dynamics decouples $(\delta z_1, \delta w_1)$ and $(\delta z_2, \delta w_2)$.

The "center of mass" dynamics $(\delta z_1, \delta w_1)$ near $y_1 = y_2 = \pi$ gives

$$\delta\dot{z}_1 = (1 - 2K)\delta w_1, \tag{52a}$$

$$\delta\dot{w}_1 = 2\sqrt{\sigma - p^*}\,\delta z_1. \tag{52b}$$

The eigenvalues are given by

$$\lambda^2 = 2\sqrt{\sigma - p^*}\left(1 - \frac{1}{2}p^{*3}\right). \tag{53}$$

They are real for $p^* < 2^{1/3}$ and imaginary for $p^* > 2^{1/3}$. Thus, the p^*_{low} solution is unstable and the p^*_{high} one is stable. The critical value $p^* = 2^{1/3}$ implies that $\sigma = 3/4^{1/3}$, in agreement with the $N = 1$ case.

For the "relative motion" $(\delta z_2, \delta w_2)$ dynamics

$$\delta\dot{z}_2 = \delta w_2, \tag{54}$$

$$\delta\dot{w}_2 = 2\sqrt{\sigma - p^*}\,\delta z_2, \tag{55}$$

the eigenvalues solve $\lambda^2 = 2\sqrt{\sigma - p^*} > 0$ and are always real. Therefore, the coinciding particle solution at $y_1 = y_2 = \pi$ with $p_1 = p_2$ is always unstable.

C. Oppositely placed particles

For the nonvanishing wave reference state, let $\theta_0 = 0$, viz., $X_0 = \sqrt{2I_0}$ and $Y_0 = 0$, $x_{10} = 0$, $x_{20} = \pi$, and $p_{10} = p_{20} = 0$. This exact solution has no analog in the $N = 1$ case. Near this state, the energy reduces to second order to

$$\delta^2 H = \frac{\delta p_1^2 + \delta p_2^2}{2} + \delta Y(\delta x_1 - \delta x_2) + X_0\frac{\delta x_1^2 - \delta x_2^2}{2}, \tag{56}$$

and momentum to first order to

$$\delta P = \delta p_1 + \delta p_2 + X_0\delta X. \tag{57}$$

The linearized evolution equations read

$$\frac{\mathrm{d}}{\mathrm{d}t}\begin{pmatrix} \delta x_1 \\ \delta p_1 \\ \delta x_2 \\ \delta p_2 \\ \delta X \\ \delta Y \end{pmatrix} = \begin{pmatrix} 0 & 1 & 0 & 0 & 0 & 0 \\ -X_0 & 0 & 0 & 0 & 0 & -1 \\ 0 & 0 & 0 & 1 & 0 & 0 \\ 0 & 0 & X_0 & 0 & 0 & 1 \\ 1 & 0 & -1 & 0 & 0 & 0 \\ 0 & 0 & 0 & 0 & 0 & 0 \end{pmatrix} \begin{pmatrix} \delta x_1 \\ \delta p_1 \\ \delta x_2 \\ \delta p_2 \\ \delta X \\ \delta Y \end{pmatrix}. \tag{58}$$

The eigenvalue 0 is degenerate, with eigenvector $(1, 0, 1, 0, 0, -X_0)^{\mathrm{T}}$ corresponding to a simple translation in space and the associated

change in the wave phase, and eigenvector $(0,0,0,0,1,0)^{\mathrm{T}}$ corresponding to a change in the wave intensity. The latter eigenvector changes P. Neither eigenvector changes H.

The eigenvalues $\lambda = \pm\sqrt{X_0}$ are simple, with eigenvectors $(0,0,\lambda,X_0,-1,0)^{\mathrm{T}}$ corresponding to particle 2 moving in the vicinity of its unstable equilibrium (conditioned by the wave). The change of momentum for particle 2 is compensated with the change of wave intensity so that these two (complex conjugate) eigenvectors lie in the plane tangent to constant (P,H) surfaces.

The eigenvalues $\lambda = \pm\mathrm{i}\sqrt{X_0}$ are simple, with eigenvectors $(\lambda,-X_0,0,0,1,0)^{\mathrm{T}}$ corresponding to particle 1 oscillating in the vicinity of its stable equilibrium (conditioned by the wave). The change of momentum for particle 1 is compensated with the change of wave intensity so that these two eigenvectors lie in the plane tangent to constant (P,H) surfaces.

In summary, the $I > 0$ solutions are unstable in six-dimensional space: they have two eigenvectors with 0 eigenvalue (cf. constants of the motion), two eigenvectors related to elliptic perturbations, and two related to hyperbolic perturbations.

The clear link between the four nonzero eigenvalues and the motion of a single particle should not obscure the fact that the wave variables (X,Y) must also evolve during these eigenmotions. Indeed, the particle–wave system is self-consistent, and one should not use blindly the stability analysis relevant to *slaved* particles (though this analysis hints at the actual self-consistent behavior).

Finally, let us recall that this analysis is formulated for the fixed point $y_1 = 0, y_2 = \pi, p_1 = p_2 = 0$. On relabeling particles, it also applies to the fixed point $y_1 = \pi$, $y_2 = 0$, and $p_1 = p_2 = 0$. In the four-dimensional phase space of the reduced model (24) with fixed total momentum P, this latter fixed point is distinct from the former one. Therefore, the stable and unstable manifolds of both fixed points will generate heteroclinic connections within their common homoclinic tangle.

VI. REGULAR AND CHAOTIC TRAJECTORIES

Chaos in the self-consistent interaction of two particles ($N = 2$) with one wave ($M = 1$) is expected since this is a non-integrable Hamiltonian system, and there is no nontrivial solution with a traveling wave.[47] Moreover, it is intuitive to think that typically chaos starts and is more intense in the regions close to the separatrix of the $N = 1$ system.[1] In particular, the explicit solution for the separatrix can be used to prove nonintegrability of perturbations of this system using the Melnikov–Poincaré integral.[50,51]

In our case, there are two standard ways for chaos to appear and grow. One is the homoclinic tangle growing from a separatrix, and the other is resonances near elliptic points, as discussed in Sec. V.

To keep the discussion simple, we consider here the case $P = 2$ so that $\sigma = 1$, and the $N = 1$ reference model has $P_{N=1} = 2^{-1/3}$. For this total momentum, the integrable $N = M = 1$ system has only one fixed point, as in Fig. 3(a).

A. Chaos near the elliptic fixed point for $H < 0$

In the negative energy regime, the wave intensity is large and the kinetic energy of the particles is low so that the particles oscillate at the bottom of the wave potential well. For a very small perturbation, the two particles "agglomerate" and move together in such a way that the evolution can be understood as if there was only one particle ($N = 1$) in the system. This dynamics is represented by the black (outer oval) trajectory in Fig. 4.

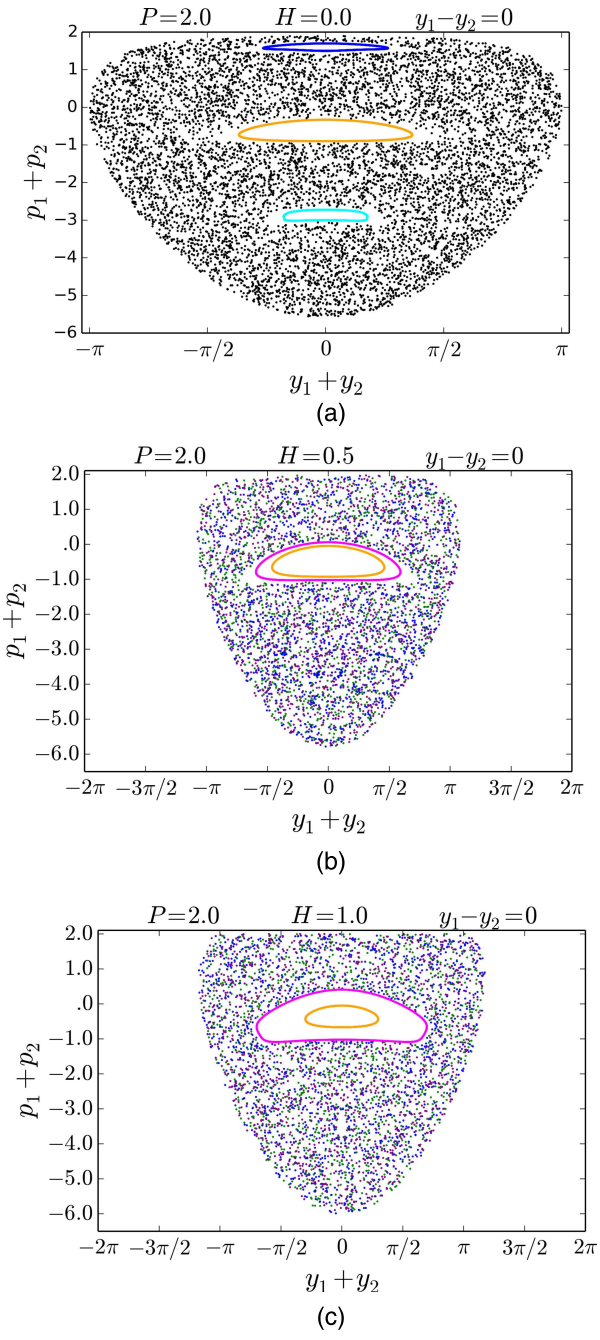

FIG. 9. Poincaré section at $y_1 - y_2 = 0$ for moderate positive H values. (a) $H = 0.0$, (b) $H = 0.5$, and (c) $H = 1.0$.

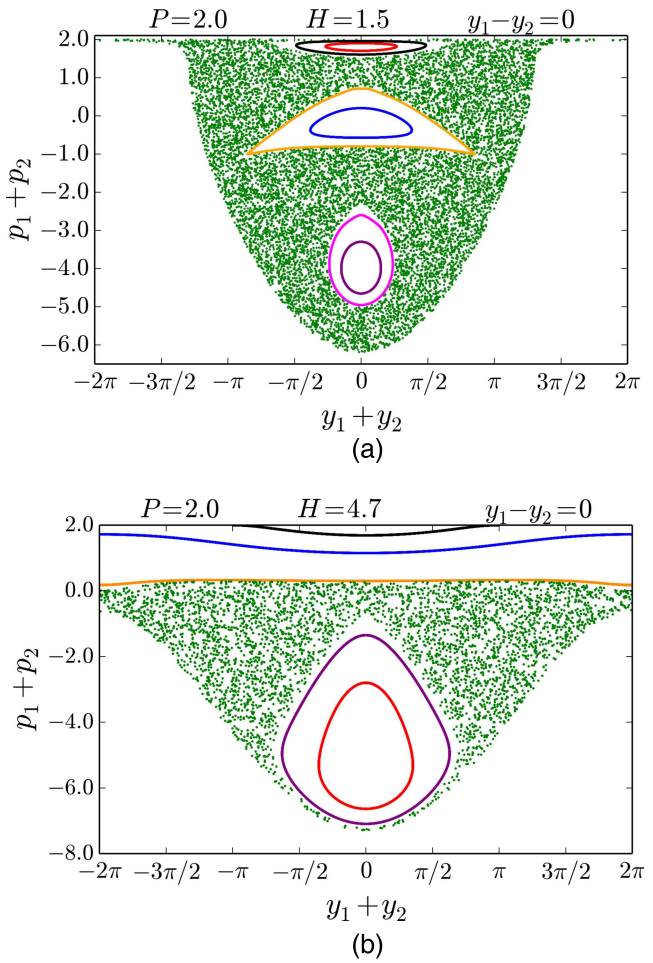

FIG. 10. Interception of trajectories with the Poincaré section located at $y_1 - y_2 = 0$ for large positive H values. The system total momentum is $P = 2$ on both panels and the total energy increases from (a) $H = 1.5$ to (b) $H = 4.7$.

The perturbation strength, which is given by the difference in the initial velocities of the particles, increases from the black (outer oval) to the blue (central point) trajectory. The outer oval trajectory corresponds to $w_2 = 0$ and $z_2 = 0$, and it remains forever in the Poincaré section plane, as we saw in Sec. IV B. The other trajectories only intersect the section plane at times at which the two particles cross each other (having then a nonzero relative velocity $2w_2$).

The Fourier transform of the particles total momentum $p_1 + p_2$ for the black (outer oval) trajectory is displayed in Fig. 5, and it shows that the system then oscillates harmonically with a single frequency.

For the blue (central point) trajectory in Fig. 4, which has the highest perturbation strength for this energy surface, we find that, as we increase the disturbance in the system, the oscillation amplitude of the particles center of mass increases and the particles start oscillating in anti-phase with respect to each other. The relative motion of the particles with respect to the wave gives rise to a resonance, as shown by the Fourier transform in Fig. 6. The contribution of this resonance is eventually enough to establish resonance overlap and chaos, as seen in Figs. 7(a) and 7(b), with (w_1, z_1) trajectories confined in the band $\cos z_1 > 0$.

This is the usual scenario near an elliptic fixed point, with deformation and destruction of tori due to increased disturbance as predicted by the KAM theorem.[52] Furthermore, the Poincaré–Birkhoff theorem predicts that when a resonant torus is destroyed (due to the increase in the perturbation), a sequence of periodic orbits will appear in phase space, which alternate between elliptic (stable) and hyperbolic (unstable), generating periodic points in the Poincaré section. In this scenario, hyperbolic points are related to the emergence of chaos while elliptic points become the center of stable regions, called resonant islands, immersed in the chaotic sea.[52] When the perturbation is increased, the trajectories that contain an unstable point [as the one similar to an "8" in Fig. 7(a)] give rise to chaos in this region.

Figures 8(a) and 8(b) show the time evolution of the particles total momentum and its Fourier transform for the dark red (similar to an "8") and the blue (chaotic) trajectories of Figs. 7(a) and 7(b), respectively. Despite the noise in the Fourier-transformed signal, the peak frequency and its harmonics still appear well defined. This may be related to the fact that when one or both particles escape from the wave potential well (giving rise to a burst of chaos), they are easily recaptured by the wave potential well. Hence, in this energy regime, the chaotic trajectory does not present a large excursion through phase space.

B. Chaos with a separatrix for $0 \le H < P^2/4$

At $H = 0$, for positive P, a new special solution appears, with particles at opposite positions (see Sec. V C). This solution is "far" from the Poincaré surface $y_1 = y_2$, and it does not significantly alter the Poincaré sections, as shown by Fig. 9(a). But its existence enables

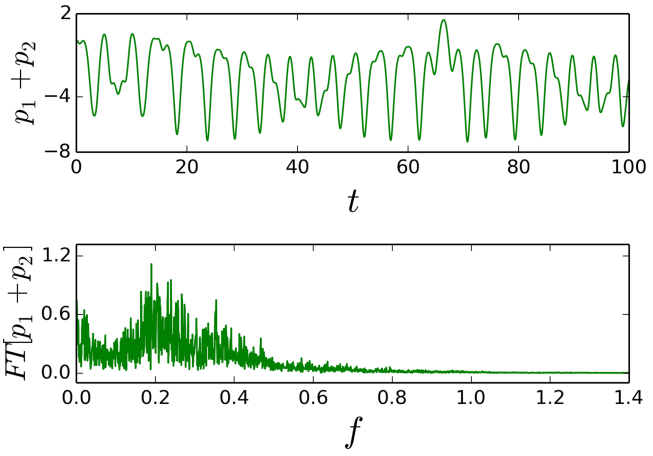

FIG. 11. Time evolution and Fourier transform of the particles total momentum for the green chaotic trajectory in Fig. 10(b).

the appearance of a connection between hyperbolic points (with one particle at the crest of the wave), which generates further chaos.

Indeed, close to a separatrix, the distances between resonances are very small so that for small perturbation values the system can be driven quickly to the chaotic regime.[51,53] In our case, in particular, this means that the dynamics becomes strongly chaotic even for small initial perturbations (z_2, w_2) of a coinciding-particles solution.

Even for larger energy, as long as $H < P^2/4$, the wave intensity cannot vanish during the system evolution. Indeed, when $I = 0$, the energy reduces to $H = (p_1^2 + p_2^2)/2 = P^2/4 + w_1^2$. Therefore, when the energy remains below the threshold $P^2/4$, the wave always keeps a finite intensity, and the motion of particles is constrained by the potential well, which is modulated smoothly with time and never disappears.

C. Large-scale chaos for $H > P^2/4$

At energy $H = P^2/4$, a new type of solution appears: the wave may vanish. Then, its phase can undergo a π-jump, and large-scale chaos does prevail, in a way similar to what was observed by Menyuk[46] and del Castillo-Negrete and Firpo.[37]

Poincaré sections for larger H values are shown in Fig. 10. In this energy regime, both particles can wander far away from the bottom of the wave potential well. In particular, for $H = 1.5$, the green (chaotic) trajectory reaches close to $p_1 + p_2 = P$ (viz., $I = 0$), allowing a very wide range of values for $y_1 = y_2$.

The time evolution of the particles' total momentum and its Fourier transform for the green chaotic trajectory in Fig. 10(b) is shown in Fig. 11. The Fourier transform looks just like a noise and it is not possible to point out a peak frequency. This may suggest that, in this chaotic regime, particles are free to move in phase space after gaining energy from the wave. The particles come back to exchange energy with the wave because the system is conservative and motions occur on compact manifolds.

VII. CONCLUSION

In this work, we analyze the regular and chaotic dynamics in the wave–particle interaction using the self-consistent Hamiltonian model.[1,2] Considering the single wave model,[27,28] we study the dynamics for $N = 1$ and $N = 2$ particles.

In the first stage, we recall the analysis[29,31,43] of the self-consistent wave–particle interaction for $N = M = 1$. As this system is integrable, its phase space presents only regular trajectories. Integrable cases are important because they provide[54] a basic understanding of the coherent structures found for large N. As observed in Sec. III B for different values of total momentum, the phase portrait topology of the $H =$ constant contours changes. For the specific value $P = 3/2$, the system has a bifurcation point at which an elliptic–hyperbolic pair of fixed points coalesce.

Bifurcation diagrams (Figs. 1 and 2) provide a clear description of the system dynamics in terms of equilibrium solutions. The analysis of the phase portrait complements the bifurcation diagrams. After the saddle-center bifurcation, a separatrix orbit appears and divides the phase portrait topology in three different domains, and the evolution of the system is different in each domain. Moreover, for the special value $P = 3/4^{1/3}$, the system has a global bifurcation by which the energy line that contains $I = 0$ passes through the hyperbolic point.

For $N = 2$, we identify and analyze the emergence of chaos in a low-dimensional system. In this scenario, the discussion about the chaotic activity can be divided into two regions of phase space, namely, close to the hyperbolic and elliptic fixed points.

The appearance and intensification of chaos in the region close to the hyperbolic fixed point is usual since, for $N = 2$, the system is non-integrable, and the homoclinic tangle generated from a separatrix in a non-integrable Hamiltonian system is a skeleton near which chaotic transport develops. Chaos in this scenario is called separatrix chaos. In this region of phase space, the system presents strong sensitivity on the initial condition so that the interaction quickly leads to chaos for small variations in the particles relative position and velocity.

On the other hand, for wave–particle systems, the appearance of chaos near the elliptic fixed point is not typically expected. For negative H, the momenta p_r associated with the particles are small, whereas the wave intensity I is large since total momentum P and total energy H are conserved quantities for this dynamics. Therefore, in the beginning, the particles should move in the wave potential well and, as we increase the disturbance in the system, the particles would have more energy to exchange with the wave while remaining trapped. Our results show that the contribution of the resonance is eventually enough to destroy tori and establish chaos in this domain. A more appropriate view of the $N = 2$ and $M = 1$ system in this regime is that of two particles coupled through an effective interaction mediated by the wave, similar to the low-energy regime of the celebrated Hénon–Heiles system.[55,56] Finally, for large enough energy, the wave intensity can occasionally vanish, which results in very efficient chaos.

The description of the wave–particle interaction in low-dimensional approximation proved to be effective in analyzing basic characteristics of the system, related to the emergence and intensification of chaos for $N = 2$. Similarly, investigating the "mirror" case of $N = 1$ particle coupled to several waves is also an important issue, which will be discussed in a separate work. However, while cases $N + M = 3$ can be thoroughly investigated, increasing the number of degrees of freedom toward the $N \gg 1$ case (and similarly $M \gg 1$) is the real challenge for a sharp understanding of the fundamental problem of the transition from dynamics to statistical behavior.[1,2,57]

ACKNOWLEDGMENTS

The authors acknowledge discussions with Dr. C. Chandre, Dr. X. Leoncini, Dr. L. H. Miranda F., Dr. T. M. Rocha Filho, and members of the équipe turbulence plasma in Marseille. They also thank anonymous reviewers for constructive comments.

The Centre de Calcul Intensif d'Aix-Marseille is acknowledged for granting access to its high performance computing resources. J.V.G. acknowledges the Coordenação de Aperfeiçoamento de Pessoal de Nível Superior (CAPES) for financing her stay at Aix-Marseille Université (AMU) under the Programa de Doutorado Sanduíche no Exterior (PDSE) (Process No. 88887.307528/2018-00) and the Conselho Nacional de Desenvolvimento Científico e Tecnológico (CNPq) for a doctoral fellowship at Universidade

Federal do Paraná (UFPR) (Process No. 166914/2017-7). M.C.d.S. acknowledges the CAPES for financing her stay at AMU under the Programa Estágio Pós-Doutoral no Exterior (Process No. 88887.307684/2018-00) and the Fundação de Amparo à Pesquisa do Estado de São Paulo (FAPESP) for a postdoctoral fellowship at Universidade de São Paulo (USP) under Grant No. 2015/05186-0 (associated with Grant No. 2018/03211-6). At the beginning of this work, Y.E. enjoyed the hospitality of the grupo controle de oscilações at USP, and R.L.V. and I.L.C. enjoyed the hospitality of the équipe turbulence plasma at AMU, with support from a COFECUB-CAPES (COFECUB - Comité Français d'Évaluation de la Coopération Universitaire et Scientifique avec le Brésil) grant (Processes COFECUB No. 40273QA-Ph908/18, and CAPES No. 88881.143103/2017-01). R.L.V. received financial support from CNPq (Process No. 301019/2019-3). I.L.C. acknowledges financial support from FAPESP under Grant No. 2018/03211-6 and CNPq under Grant Nos. 407299/2018-1 and 302665/2017-0.

DATA AVAILABILITY

The data that support the findings of this study are available from the corresponding author upon reasonable request.

REFERENCES

[1]Y. Elskens and D. Escande, *Microscopic Dynamics of Plasmas and Chaos* (IOP Publishing, Bristol, 2003).
[2]D. F. Escande and Y. Elskens, "Microscopic dynamics of plasmas and chaos: The wave-particle interaction paradigm," Plasma Phys. Control. Fusion **45**, A115–124 (2003).
[3]D. G. Swanson, *Plasma Kinetic Theory* (CRC Press, Boca Raton, 2008).
[4]T. H. Stix, *Waves in Plasmas* (Springer-Verlag, New York, 1992).
[5]C. F. F. Karney and A. Bers, "Stochastic ion heating by a perpendicularly propagating electrostatic wave," Phys. Rev. Lett. **39**, 550–554 (1977).
[6]G. R. Smith and N. Pereira, "Phase-locked particle motion in a large-amplitude plasma wave," Phys. Fluids **21**, 2253–2262 (1978).
[7]R. Balescu, *Transport Processes in Plasmas* (North-Holland, Amsterdam, 1988).
[8]S. Ichimaru, *Statistical Plasma Physics, Vol. I: Basic Principles* (CRC Press, Boca Raton, 2018).
[9]Y. Elskens, "Irreversible behaviours in Vlasov equation and many-body Hamiltonian dynamics: Landau damping, chaos and granularity," in *Topics in Kinetic Theory, Toronto, 24 March–2 April 2004*, Fields Institute Communications Series Vol. 46, edited by T. Passot, C. Sulem, and P. L. Sulem (American Mathematical Society, Providence, 2005), pp. 89–108.
[10]N. Besse, Y. Elskens, D. F. Escande, and P. Bertrand, "Validity of quasilinear theory: Refutations and new numerical confirmation," Plasma Phys. Control. Fusion **53**, 025012 (2011).
[11]Y. Elskens, "Gaussian convergence for stochastic acceleration of particles in the dense spectrum limit," J. Stat. Phys. **148**, 591–605 (2012).
[12]A. V. Timofeev, "Cyclotron oscillations of plasma in an inhomogeneous magnetic field," Sov. Phys. Uspekhi **16**, 445 (1974).
[13]D. F. Escande, D. Bénisti, Y. Elskens, D. Zarzoso, and F. Doveil, "Basic microscopic plasma physics from *N*-body mechanics," Rev. Mod. Plasma Phys. **2**, 9 (2018).
[14]F. Doveil, D. F. Escande, and A. Macor, "Experimental observation of nonlinear synchronization due to a single wave," Phys. Rev. Lett. **94**, 085003 (2005).
[15]F. F. Chen, *Introduction to Plasma Physics and Controlled Fusion* (Plenum Press, New York, 1984).Vol. 1.
[16]W. Herr, "Introduction to Landau damping," in *Advanced Accelerator Physics, Trondheim, 19–29 August 2013*, edited by W. Herr (CERN, Geneva, 2014).
[17]J. He, L. Wang, C. Tu, E. Marsch, and Q. Zong, "Evidence of Landau and cyclotron resonance between protons and kinetic waves in solar wind turbulence," Astrophys. J. Lett. **800**, L31 (2015).
[18]C. H. K. Chen, K. G. Klein, and G. G. Howes, "Evidence for electron landau damping in space plasma turbulence," Nat. Commun. **10**, 1–8 (2019).
[19]L. D. Landau, "On the vibrations of the electronic plasma," Yad. Fiz. **10**, 25 (1946).
[20]D. D. Ryutov, "Landau damping: Half a century with the great discovery," Plasma Phys. Control. Fusion **41**(3A), A1–A12 (1999).
[21]P. Stubbe and A. I. Sukhorukov, "On the physics of Landau damping," Phys. Plasmas **6**, 2976–2988 (1999).
[22]Y. Elskens, D. F. Escande, and F. Doveil, "Vlasov equation and *N*-body dynamics: How central is particle dynamics to our understanding of plasmas?," Eur. Phys. J. D **68**, 1–7 (2014).
[23]D. F. Escande, "Stochasticity in classical Hamiltonian systems: Universal aspects," Phys. Rep. **121**, 165–261 (1985).
[24]M. C. de Sousa, F. M. Steffens, R. Pakter, and F. B. Rizzato, "Standard map in magnetized relativistic systems: Fixed points and regular acceleration," Phys. Rev. E **82**, 026402 (2010).
[25]Y. H. Ichikawa, T. Kamimura, and C. F. F. Karney, "Stochastic motion of particles in tandem mirror devices," Physica D **6**, 233–240 (1983).
[26]H. E. Mynick and A. N. Kaufman, "Soluble theory of nonlinear beam-plasma interaction," Phys. Fluids **21**, 653–663 (1978).
[27]I. N. Onishchenko, A. R. Linetskii, N. G. Matsiborko, V. D. Shapiro, and V. I. Shevchenko, "Contribution to the nonlinear theory of excitation of a monochromatic plasma wave by an electron beam," Soviet Phys. JETP **11**, 281–285 (1971).
[28]T. M. O'Neil, J. H. Winfrey, and J. H. Malmberg, "Nonlinear interaction of a small cold beam and a plasma," Phys. Fluids **14**, 1204–1212 (1971).
[29]J. L. Tennyson, J. D. Meiss, and P. J. Morrison, "Self-consistent chaos in the beam-plasma instability," Physica D **71**, 1–17 (1994).
[30]A. Antoniazzi, Y. Elskens, D. Fanelli, and S. Ruffo, "Statistical mechanics and Vlasov equation allow for a simplified Hamiltonian description of single-pass free electron laser saturated dynamics," Eur. Phys. J. B **50**, 603–611 (2006).
[31]J. C. Adam, G. Laval, and I. Mendonça, "Time-dependent nonlinear Langmuir waves," Phys. Fluids **24**, 260–267 (1981).
[32]M.-C. Firpo and Y. Elskens, "Kinetic limit of N-body description of wave-particle self-consistent interaction," J. Stat. Phys. **93**, 193–209 (1998).
[33]N. Carlevaro, G. Montani, and D. Terzani, "On the viability of the single-wave model for the beam plasma instability," Europhys. Lett. **115**, 45004 (2016).
[34]M.-C. Firpo and Y. Elskens, "Phase transition in the collisionless damping regime for wave-particle interaction," Phys. Rev. Lett. **84**, 3318–3321 (2000).
[35]N. A. Yampolsky and N. J. Fisch, "Simplified model of nonlinear Landau damping," Phys. Plasmas **16**, 072104 (2009).
[36]Z. Huang and K.-J. Kim, "Review of x-ray free-electron laser theory," Phys. Rev. ST Accel. Beams **10**, 034801 (2007).
[37]D. del Castillo-Negrete and M.-C. Firpo, "Coherent structures and self-consistent transport in a mean field Hamiltonian model," Chaos **12**, 496–507 (2002).
[38]D. Testa, A. Fasoli, D. Borba, M. de Baar, M. Bigi, J. Brzozowski, P. de Vries, JET-EFDA Contributors *et al.*, "Alfvén mode stability and wave-particle interaction in the JET tokamak: Prospects for scenario development and control schemes in burning plasma experiments," Plasma Phys. Control. Fusion **46**, S59–S79 (2004).
[39]E. Hairer, C. Lubich, and G. Wanner, *Geometric Numerical Integration: Structure-preserving Algorithms for Ordinary Differential Equations* (Springer, Berlin, 2006).
[40]G. M. Zaslavsky, *Hamiltonian Chaos and Fractional Dynamics* (Oxford University Press, New York, 2005).
[41]J. D. Crawford and A. Jayaraman, "First principles justification of a "single wave model" for electrostatic instabilities," Phys. Plasmas **6**, 666–673 (1999).
[42]D. Farina, F. Casagrande, U. Colombo, and R. Pozzoli, "Hamiltonian analysis of the transition to the high-gain regime in a Compton free-electron-laser amplifier," Phys. Rev. E **49**, 1603–1609 (1994).
[43]D. del Castillo-Negrete, "Dynamics and self-consistent chaos in a mean field Hamiltonian model," in *Dynamics and Thermodynamics of Systems with Long-Range Interactions, Les Houches, 18–22 February 2002*, edited by T. Dauxois, S. Ruffo, E. Arimondo, and M. Wilkens (Springer, Berlin, 2002), pp. 407–436.

[44]A. V. Bolsinov, A. V. Borisov, and I. S. Mamaev, "Topology and stability of integrable systems," Russian Math. Surveys **65**, 259–318 (2010).
[45]A. H. Boozer, "Arnold diffusion and adiabatic invariants," Phys. Lett. A **185**, 423–427 (1994).
[46]C. R. Menyuk, "Particle motion in the field of a modulated wave," Phys. Rev. A **31**, 3282–3290 (1985).
[47]Y. Elskens, "Finite-*N* dynamics admit no travelling-waves solutions for the Hamiltonian *XY* model and single-wave collisionless plasma model," in *ESAIM: Proceedings* (EDP Sciences, 2001), Vol. 10, pp. 221–215.
[48]D. F. Escande, S. Zekri, and Y. Elskens, "Intuitive and rigorous microscopic description of spontaneous emission and Landau damping of Langmuir waves through classical mechanics," Phys. Plasmas **3**, 3534–3539 (1996).
[49]J. D. Meiss, *Differential Dynamical Systems* (SIAM, Philadelphia, 2017).
[50]V. Kozlov, "Integrability and non-integrability in Hamiltonian mechanics," Russ. Math. Surveys **38**, 1–76 (1983).
[51]J. Guckenheimer and P. Holmes, *Nonlinear Oscillations, Dynamical Systems, and Bifurcations of Vector Fields* (Springer, New York, 1983).
[52]E. Ott, *Chaos in Dynamical Systems* (Cambridge University Press, 2002).
[53]A. J. Lichtenberg and M. A. Lieberman, *Regular and Stochastic Motion* (Springer, New York, 1983).
[54]R. Pakter and G. Corso, "Improving regular acceleration in the non-linear interaction of particles and waves," Phys. Plasmas **2**, 4312–4324 (1995).
[55]M. Hénon and C. Heiles, "The applicability of the third integral of motion: Some numerical experiments," Astron. J. **69**, 73 (1964).
[56]J. H. Lowenstein, *Essentials of Hamiltonian Dynamics* (Cambridge University Press, Cambridge, 2012).
[57]Y. Elskens and C. Firpo, "Kinetic theory and large-N limit for wave-particle self-consistent interaction," Phys. Scripta **T75**, 169–172 (1998).